CLO

WHEEL FAILURE MECHANISMS OF RAILROAD CARS

FINAL REPORT

Volume 1
(Summary Report)

FRA Contract Number DTFR53-82-C-00282, Task Order #6

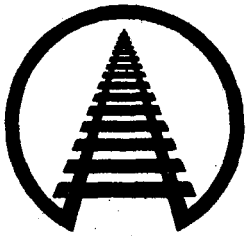

Association of American Railroads

Britto R. Rajkumar
Transportation Test Center
Pueblo, Colorado
&
Daniel H. Stone
AAR Technical Center
Chicago, Illinois

03 - Rail Vehicles & Components

ASSOCIATION OF AMERICAN RAILROADS
RESEARCH AND TEST DEPARTMENT

WHEEL FAILURE MECHANISMS OF RAILROAD CARS
VOLUME I - FINAL SUMMARY REPORT

Report No. R-679

B. R. RAJKUMAR
D. H. STONE

Contract No. DTFR53-82-C-00282

November, 1987

AAR Transportation Test Center
Pueblo, Colorado 81001

DISCLAIMER

This report is disseminated by the AAR for informational purposes only and is given to, and accepted by, the recipient at its sole risk. The AAR and the FRA make no representations or warranties, either express or implied, with respect to the report or its contents. The AAR and the FRA assume no liability to anyone for special, collateral, exemplary, indirect, incidental, consequential or any other kind of damage resulting from the use or application of this report or its content. Any attempt to apply the information contained in this paper is done at the recipient's own risk.

1. REPORT NO.	2. REPORT DATE	3. PERIOD COVERED
R-679 - Volume I	November, 1987	September, 1983 - January, 1987

4. TITLE AND SUBTITLE

Wheel Failure Mechanisms of Railroad Cars
Volume I - Final Summary Report

5. AUTHOR(S)

Britto R. Rajkumar, Section Manager
Daniel H. Stone, Director - Metallurgy

6. PERFORMING ORGANIZATION NAME AND ADDRESS

Association of American Railroads
Transportation Test Center
P. O. Box 11130
Pueblo, Colorado 81001

7. TYPE OF REPORT

8. CONTRACT OR GRANT NO.

DTFR53-82-C-00282

9. SPONSORING AGENCY NAME AND ADDRESS

United States Department of Transportation
Federal Railroad Administration
400 7th Street, S. W.
Washington, D. C. 20590

10. NO. OF PAGES

97

11. NO. OF REFERENCES

12

12. SUPPLEMENTARY NOTES

FRA Task Order 6 - Final Report

13. ABSTRACT

This report summarizes an extensive research program into the causes of wheel thermal failure. Results of material property tests, review of failure data, dynamometer tests, roll dynamics unit, track tests, and theoretical and experimental stress analysis show that heat-treated wheels of designs which meet the requirements of AAR Standard S.660 (low-stress wheels) are significantly more resistant to failure.

Volume I presents a summary of the data and results, while Volume II gives a detailed reporting of each of the technical tasks undertaken in the completion of the program. Volume III is an appendix of highly detailed research data.

14. SUBJECT TERMS

Residual Stress, Thermal Cracking, Wheel Failure, Wheel Steel Fatigue, Wheel Stress Analysis, Wheels

15. AVAILABILITY STATEMENT

Assistant Vice President
Association of American Railroads
Technical Center
3140 South Federal Street
Chicago, Illinois 60616

EXECUTIVE SUMMARY

This report presents the results of an extensive study into the causes of thermally induced wheel failure. Major issues addressed include the effects of wheel plate design, heat-treatment, ability to resist thermal damage, the relationship between discoloration and residual stress reversal, and the amount of brake energy required to cause changes in the residual stress in a wheel.

Results of this study show that heat-treated, curved plate (low stress) wheels are the most resistant to thermal and mechanical damage and, therefore, resistant to failure.

A survey of wheel performance was made using data based on wheel removals and derailments. Results of this study indicate that derailments due to thermally induced wheel failure are highly seasonal, with the majority of failures occurring during the winter months. The number of derailments due to thermally induced wheel failure has declined significantly over the last seven years as have all other categories of derailments. It was found that mechanical damage (i.e. tread metal flow, excessive wear, metallurgical transformation) is necessary for the initiation of thermal cracks and thus failure. Further, derailment data show that wheels with curved plate designs are several times less likely to fail than wheels of straight plate design; lack of population and mileage data for heat-treated wheels preclude use of derailment data to assess the role of heat-treatment in failure rate.

Additional information was gathered from an extensive program of saw cutting wheels that had been in service. Experimental programs were conducted using a dynamometer, the roll-dynamics unit, and on-track testing. Heat-treated curved plate wheels are more resistant to both stress-reversal and mechanical damage than any other combination of design and heat-treatment, and therefore more resistant to thermally induced failure. Over-hanging brake shoes and non-uniform tread heating were found to be conditions which will increase the probability of wheel failure.

Specific combinations of speed, time and brake shoe force are required to produce thermal damage in the rim for each wheel design and heat-treatment. These data should be used to promote brake system performance specifications.

It was found that discoloration*, while it indicates thermal input, is not necessarily evidence of destructive thermal damage. Discoloration indicates a greater probability of an adverse change in residual stress. However, it should be noted that research indicates some nondiscolored wheels may have developed high residual tensile stresses. The following diagram presents the schematic distribution of wheel population and illustrates that the derailment rate is higher for discolored wheels than nondiscolored wheels, while the absolute number of derailments is higher for nondiscolored wheels.

---

*Discoloration is defined as "a pattern of 'reddish brown' or 'blue' discoloration from heat on front and back face of rim, 4-inches into the plate with decreasing intensity."

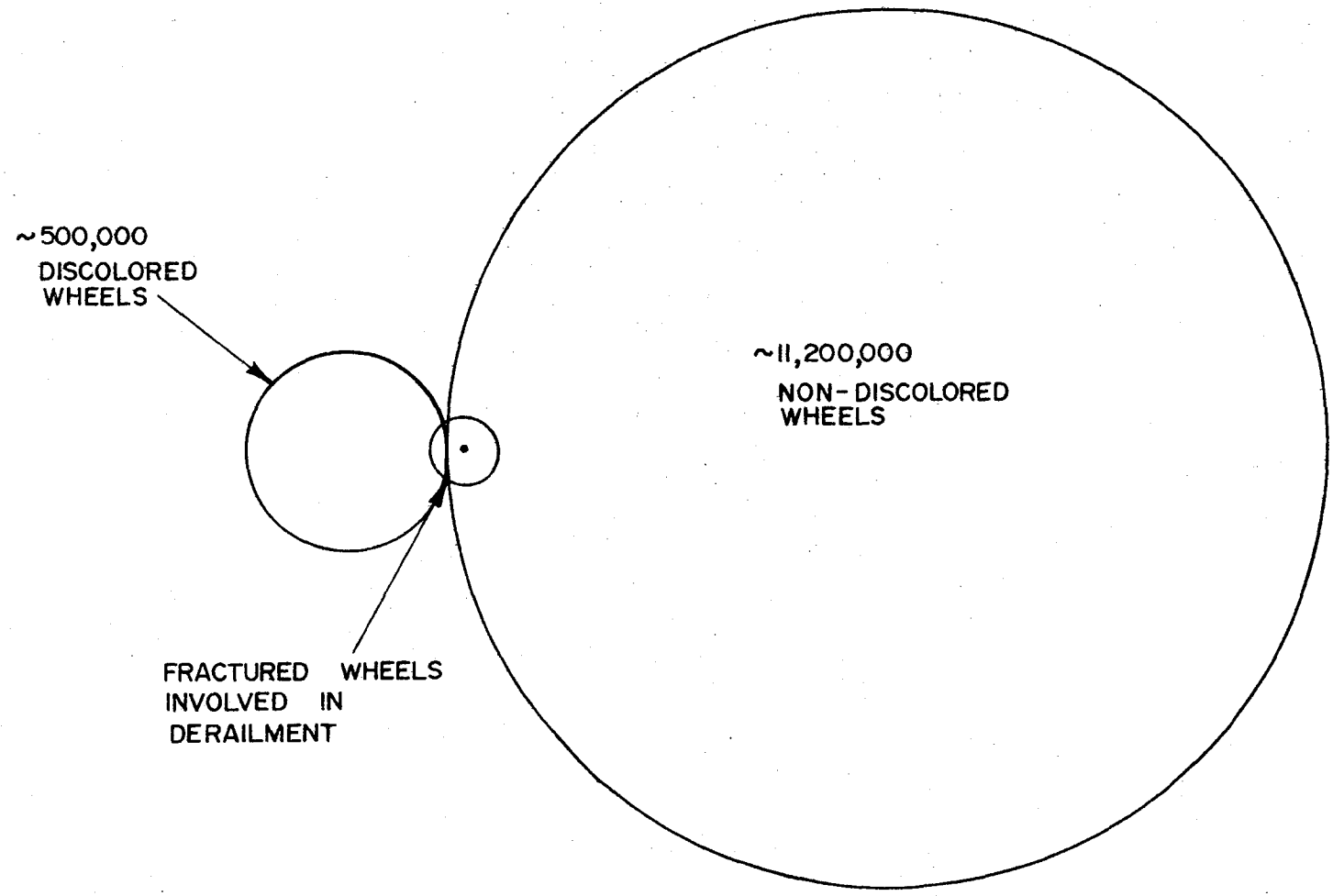

SCHEMATIC DISTRIBUTION OF WHEEL POPULATION

TABLE OF CONTENTS

LIST OF FIGURES

LIST OF FIGURES (Contd.)

LIST OF FIGURES (Contd.)

LIST OF TABLES

1.0 INTRODUCTION

The life of a railroad wheel is determined by various factors such as wear, plastic flow, fatigue failure of the wheel plate, shelling and thermal cracking, and wheel fracture. The incidence of heat related wheel failure, which is initiated by a thermal crack in the wheel rim, has become of great importance in the railroad industry. In order to reduce the likelihood of this type of failure, a large number of wheels are removed from service on the basis of the discoloration* of the wheel plate, caused, presumably, by severe thermal loads. The discolored wheels are thought to have high residual stress which could lead to thermal crack failure. The problem of identifying a thermally abused wheel in service is very complex. Research has shown that some wheels may develop high levels of residual tensile stress in the rim. These stress levels can promote the propagation of radial rim cracks and eventually contribute to catastrophic wheel failures. Research has also indicated that the initial residual stresses in the rim are altered by the complex effect of thermal stresses due to severe modes of braking operation. Additionally, the effect of alternating stresses due to the mechanical loads at the wheel/rail interface are not well understood.

In general, the wheel thermal failure problem presents the following questions which this report will attempt to answer.

---

*Discoloration is defined as "a pattern of 'reddish brown' or 'blue' discolorations from heat on front and back face of rim, 4-inches into the plate with decreasing intensity."

1. What effect does wheel plate design have on the wheel's ability to resist fracture?
2. What effect does heat treating have with respect to the wheel's ability to resist fracture?
3. What is the relationship between plate discoloration and the presence of a high level of rim circumferential tensile stress?
4. How much brake energy can a wheel absorb before residual tensile stresses are induced in the rim?

A better understanding of these questions is now available as the result of this FRA sponsored Wheel Failure Mechanisms Program and other concurrent research.

The main emphasis of this effort is to understand more fully the mechanisms of wheel failure and to develop technically sound wheel-removal criteria and guidelines for safe operation. The scope of the program progresses from a technology survey, through a national study of wheel removal guidelines, to individual technical problem-oriented tasks that include laboratory and track testing and analyses. A review of the major findings of this program follows.

2.0 THE WHEEL FAILURE ENVIRONMENT (LESSONS FROM FIELD EXPERIENCE)

2.1 Wheel Failure and Removal Data

The removal and failure trends of railroad freight car wheels was monitored to characterize wheel failure patterns developing in service. The methods used and the data sources of information chosen were:

1. The AAR Car Repair Billing System Data Base,

2. The AAR Wheel Failure Report Data Base,

3. The FRA Accident-Incident Reports Data Base, and

4. The AAR Car Maintenance Cost Data Base.

Unfortunately, each of these data bases suffers from the lack of information on type of service, wheel population characteristics, and in some cases, mileage.

The method used to monitor the wheel removal and failure patterns is the control chart. The control charts have been established with control limits for one quarter, two consecutive quarters and three consecutive quarters. One control chart has been established for each combination of data source and normalizing factor (car miles, active cars or ton miles). The control limits have been established to provide 95% confidence such that when the data source mean has shifted significantly, the limits have been exceeded.

Figure 1 shows the trend for the rate of wheel removals due to discoloration (why made code 89 from Field Manual of the AAR Interchange Rules) per billion ton miles. The rate of removal for this cause has decreased significantly since the 1985 rule change requiring discoloration on both sides of the wheel.

The rate of wheel removals per billion ton miles due to thermal damage is shown in Figure 2.

The why made codes from the Field Manual of the AAR Interchange Rules are:

-- 66-flange cracked or broken,

-- 68-rim cracked or broken,

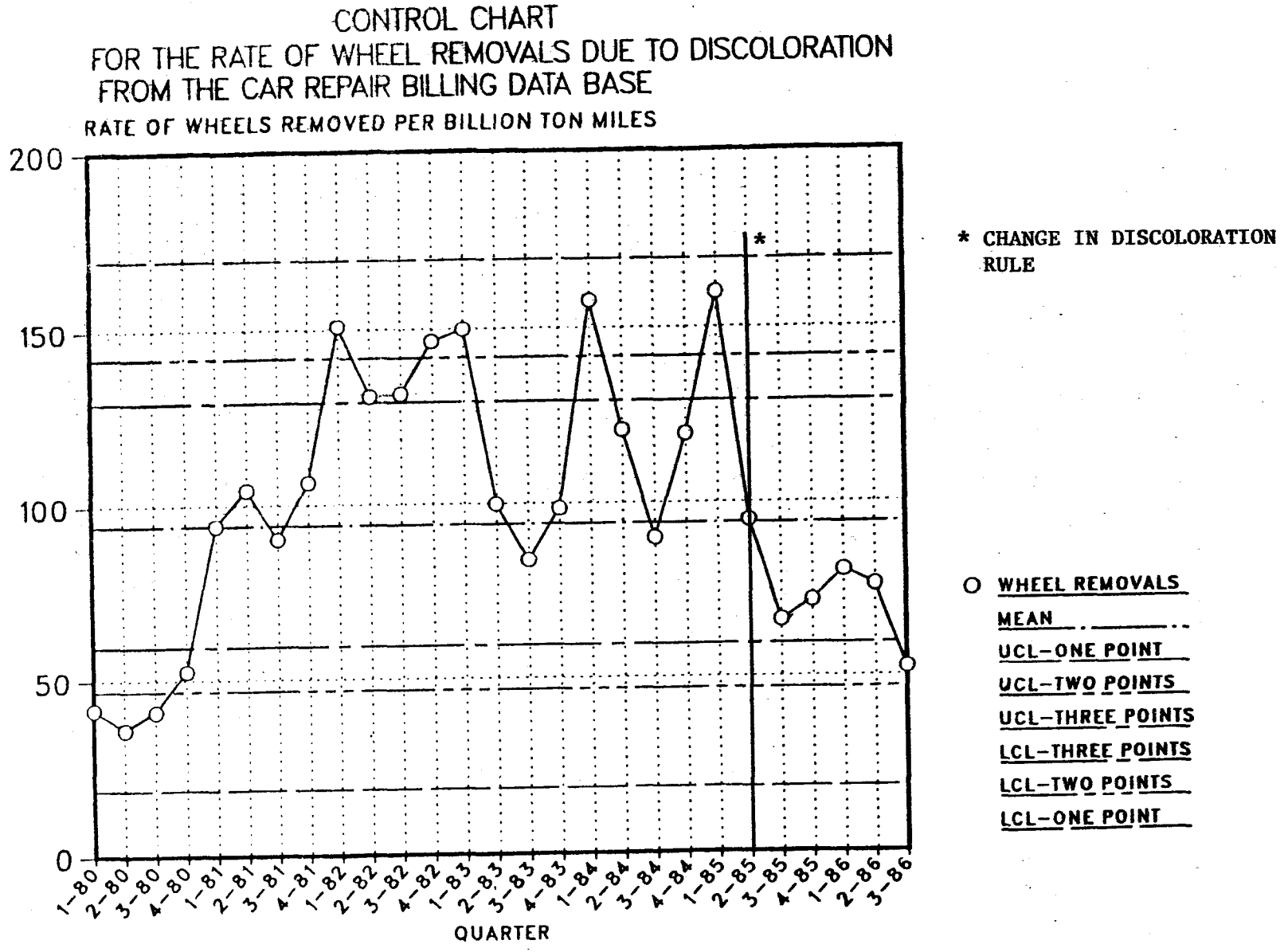

FIGURE 1 RATE OF WHEEL REMOVALS PER BILLION TON MILES DUE TO DISCOLORATION

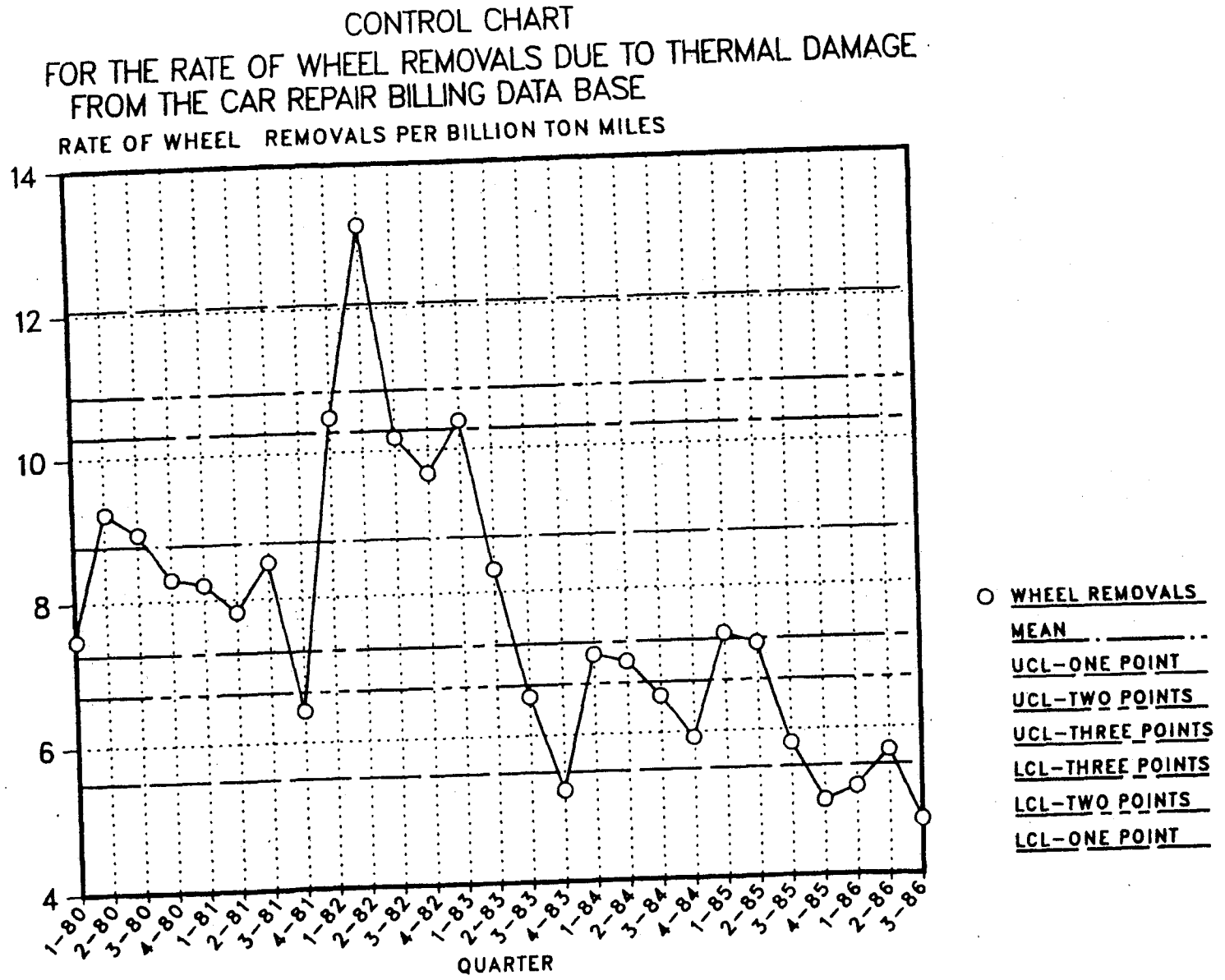

FIGURE 2 RATE OF WHEEL REMOVALS PER BILLION TON MILES DUE TO THERMAL DAMAGE

-- 69-thermal cracks with overheating,

-- 74-thermal cracks, and

-- 83-cracked or broken plate.

This chart indicates an average of approximately 9 wheels removed per billion ton miles per quarter due to thermal damage. The rate of wheel removals due to thermal damage does not show any obvious trends.

Wheel removals on account of discolored wheels and removals on account of cracked wheels do not seem to exactly move with each other. It should also be noted that the rate of removal for discoloration is approximately ten times that of wheels removed for cracking.

The trend in the rate of FRA reportable accidents caused by thermally damaged wheels is shown in Figure 3. The rate of accidents due to thermally damaged wheels has declined steadily since 1980, as have other categories of derailment. This trend has continued through 1986.

There is also a clear seasonal pattern to the derailment data with the number of derailments peaking during the winter quarter to produce approximately as many derailments as occur in the remaining nine months. It is suggested that there are probably two major reasons for this behavior: 1) the increase in brake system malfunctions due to low-temperatures, and 2) the increased track modulus due to roadbed freezing.

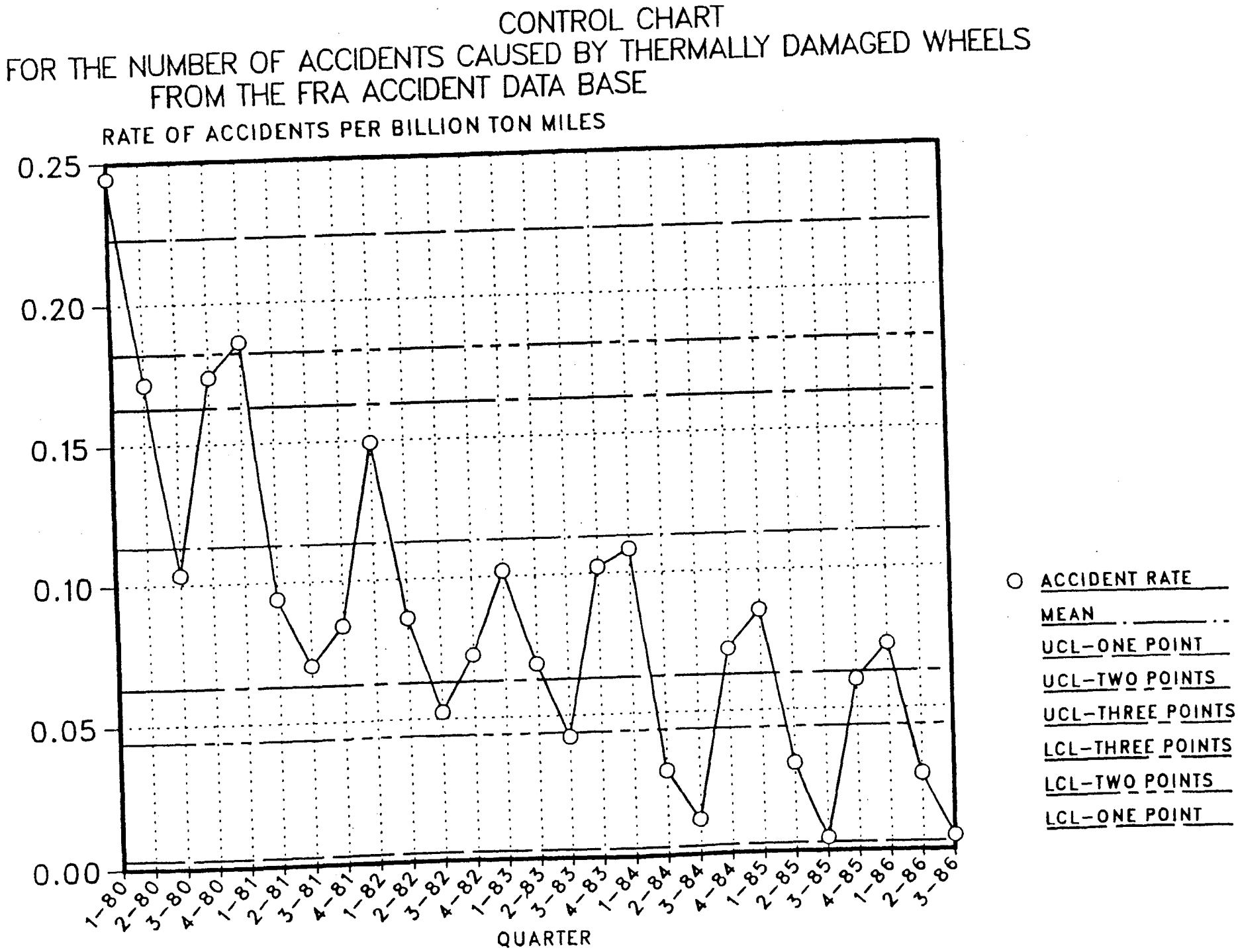

FIGURE 3 RATE OF ACCIDENTS PER BILLION TON MILES DUE TO THERMALLY DAMAGED WHEELS

The AAR MD-115 (Wheel Failure Report) forms provide a useful data base through which the associations of wheel design, discoloration, and heat-treatment can be isolated. Data on a total of 210 derailments for which MD-115 forms were submitted were gathered for the years 1983 to 1986 and have been sorted by discoloration, plate design, and heat treatment. These data are represented graphically in Figure 4, but no attempt has been made to normalize them to the existing wheel population and usage.

It is possible to use this information to make qualitative comparisons of wheel failure rates for different categories of wheels. Table 1 summarizes this information. The table is based on the analysis of 157 wheel failures in 1984 and 1985. As indicated in the table, it is estimated that there were 411 billion wheel miles in this period so that the overall wheel failure rate can be estimated at 38 failures per 100 billion wheel miles. As only 28 of the 157 wheel failures involved curved-plate wheels, it is obvious that the wheel failure rate for curved-plate wheels is significantly less than for straight-plate wheels because curved-plate wheel miles substantially exceed straight-plate wheel miles, inasmuch as they are generally on newer, more active cars.

The table also shows a breakdown for discolored and nondiscolored wheels in both the straight- and curved-plate categories. Note that for each of these wheel types the discolored wheels represent about 1/3 of the failures. Since discolored wheel miles must be much less than non-discolored

Class C, Straight Plate

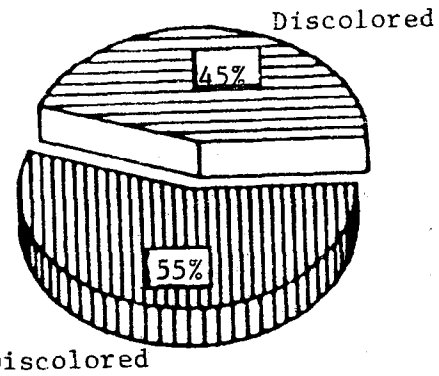

Total Wheels: 40

Class U, Straight Plate

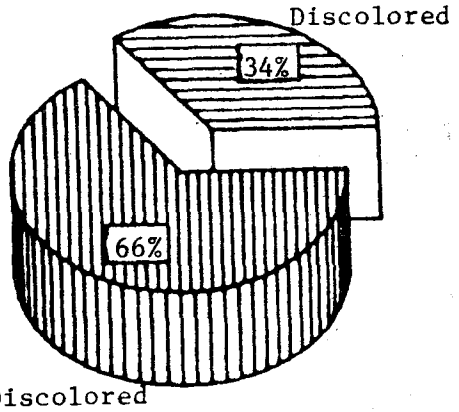

Total Wheels: 89

Class C, Curved Plate

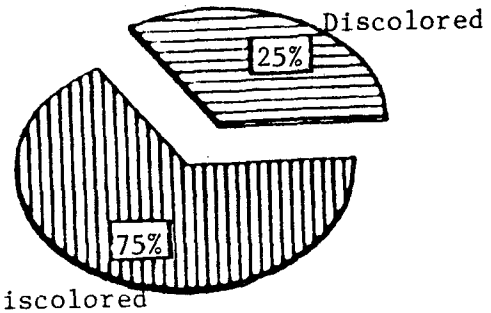

Total Wheels: 8

Class U, Curved Plate

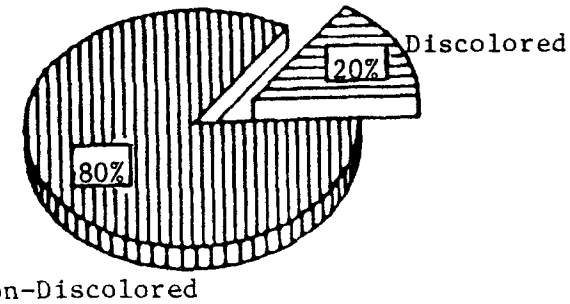

Total Wheels: 20

FIGURE 4 DISTRIBUTION OF WHEELS CAUSING DERAILMENTS BY DESIGN AND HEAT-TREATMENT

TABLE 1

WHEEL FAILURE DATA FOR CURVED-PLATE AND STRAIGHT-PLATE, DISCOLORED AND NONDISCOLORED, RAILROAD CAR WHEELS FROM AAR DATA BASE (1) (1984 AND 1985 DATA)

Condition	Wheel Failures							
Overall Failure Rate (2)	157/411 = 38 failures per 100 billion wheel miles							
	Curved-Plate				Straight-Plate			
Curved-Plate, Straight-Plate Breakdown	28				129			
	NonDiscolored		Discolored		NonDiscolored		Discolored	
NonDiscolored, Discolored Breakdown	22		6		81		48	
	B&C	U	B&C	U	B&C	U	B&C	U
Heat Treatment Breakdown	6	16	2	4	22	59	18	30

(1) Wheel failures in period include:

22	curved-plate nondiscolored wheels
6	curved-plate discolored wheels
81	straight-plate nondiscolored wheels
48	straight-plate discolored wheels
157	total wheel failures

(2) 411 billion wheel miles based on 922 billion ton miles in 1984 and 884 billion ton miles in 1985; 34.9 and 35.4 (estimated) ton miles per car mile in 1984 and 1985 respectively; and 8 wheel miles per car mile.

wheel miles (a survey done by the Union Pacific Railroad in 1983 concluded that 4.8% of the 12,000 wheels surveyed had more than 4 inches of discoloration), it is obvious that the wheel failure rate for discolored wheels must be larger than for non-discolored wheels.

The table also shows the breakdown in wheel failures by heat treatment. Because the number of failures is small, it is difficult to develop any discernible trends from the data. However, lacking data on the heat-treated vs. non-heat treated wheel population and mileage, no conclusions on the effectiveness of heat-treated wheels in resisting fracture can be drawn. The benefits of heat-treated wheels will be supported by other evidence to follow.

2.2 Description of Fracture Critical Cracks

The final set of service data reviewed are 600 railroad wheel failure analysis reports from the Union Pacific, Santa Fe, and Norfolk Southern Railroads.[1,2]* Special attention was given to approximately 400 reports that provided a sufficiently complete description of facts to permit a reliable failure analysis. These are cited in this section as "good file data".

The data from the Union Pacific cover the period for 1969 to 1983; for the Santa Fe from 1977 to 1985; and for the Norfolk Southern from 1981 to 1985.

---

*See list of references

Fracture critical cracks (FCC) are described in the failure analysis reports prepared by the individual railroad as the cracks which caused fracture resulting in a derailment.

Figure 5 describes the crack locations, relative percentage, and the typical causes for cracks studied by the Union Pacific and the Santa Fe railroads. Metallurgical examination (cross sectioning and etching adjacent to the fracture surface) established those cases in which there were hard-brittle spots due to localized surface overheating (in excess of 1350^{o} F), which produced martensite and a larger surrounding zone of spheroidized pearlite.

Figure 5 also presents a summary of crack types and metal damage. The Figure 5 codes of typical severe metal damage means that over 80 to 90% of the cases (for each crack location), involved severe metal damage as cited in the failure analysis reports.

Back rim cracks initiated, in most cases, at rim stamping are due to retarder shoe and/or guard rail action. The prohibition by AAR of rim stamping at critical locations has reduced this cause of failures.

The high percentage of inner flange cracks observed, is due to sharp points at the top of the inner face of the flange. These points are a result of the planing off of the flange, and the development of a straight metal surface that intersects the top of the flange at a sharp point. In over 90% of the inner-flange crack cases, the crack had originated at this sharp point as shown in Figure 6.

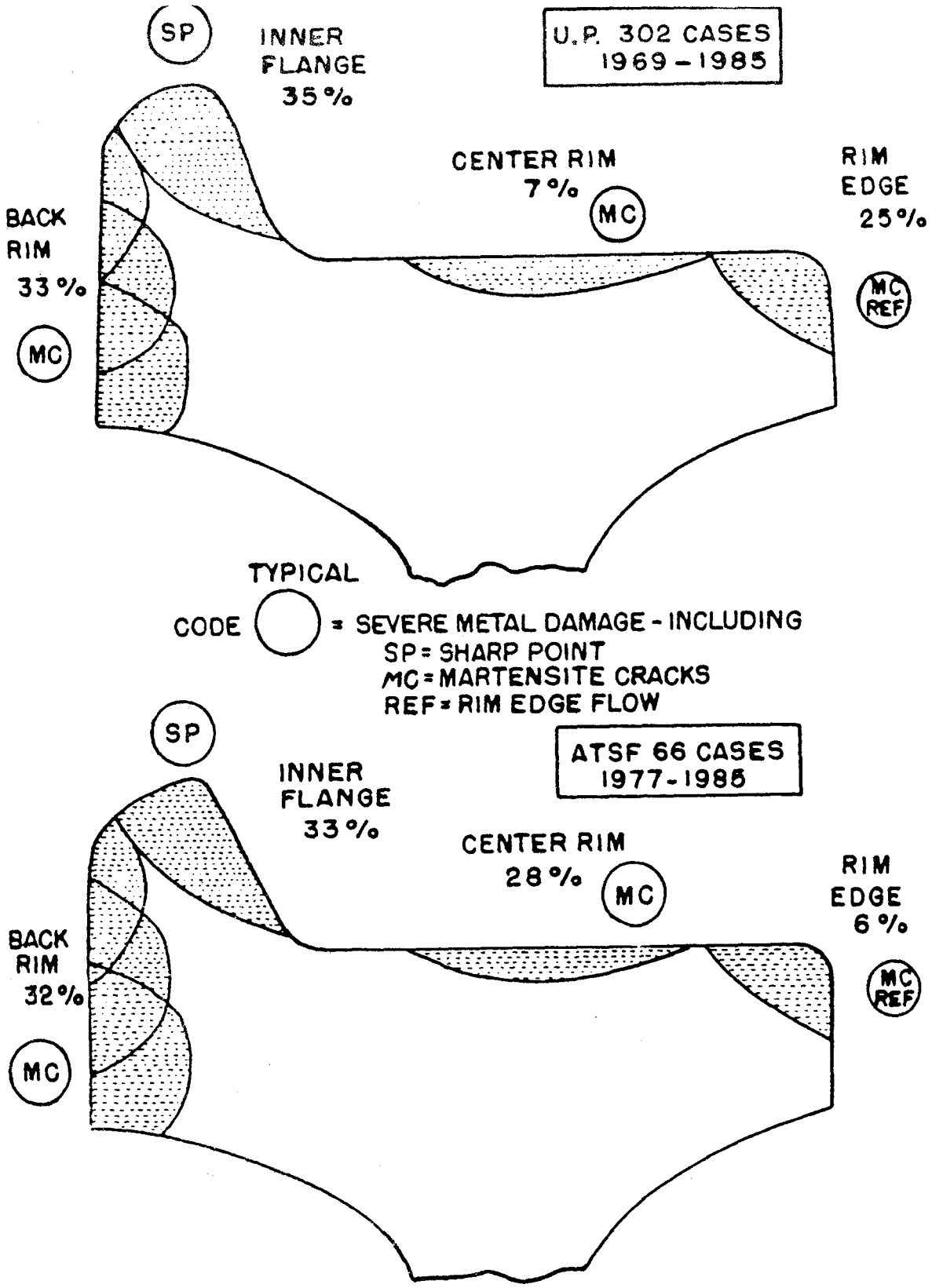

FIGURE 5 LOCATION AND FREQUENCY OF THERMAL CRACKS REMOVED FROM UNION PACIFIC AND SANTA FE RAILROADS

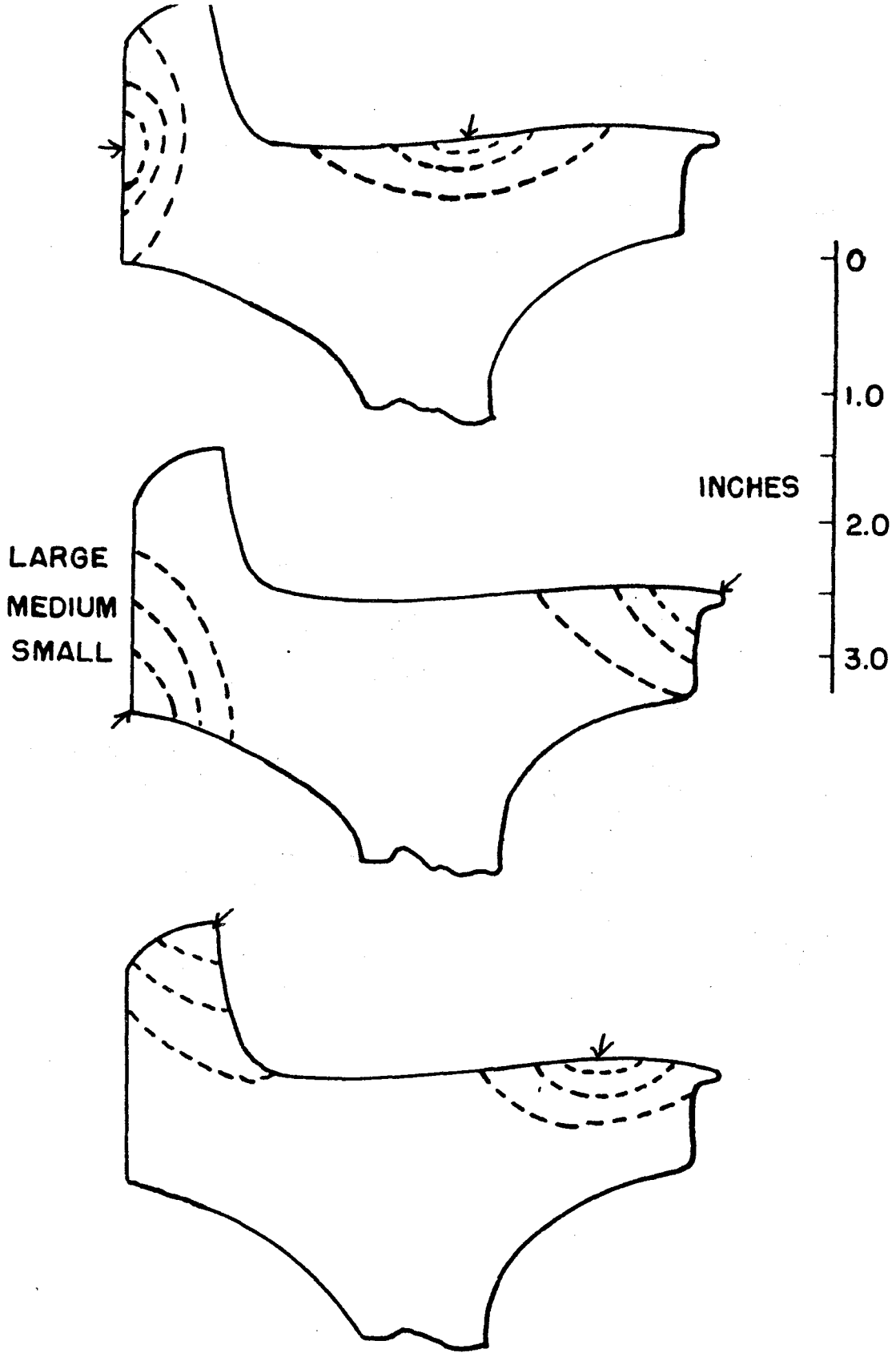

FIGURE 6 RANGE OF FRACTURE CRITICAL CRACK SIZES RESULTING IN DERAILMENTS. ARROWS INDICATE CRACK ORIGIN.

It is interesting to note that there is a significant difference in fracture behavior between straight and curved plate wheels. Virtually none of the failures of curved plate wheel originated at rim cracks. The point of crack initiation for these wheels was at the intersection of the planed metal surface and the flange. This sharp point was the site of high stress concentration and cold working which led to development of a fatigue crack and ultimate failure even in these wheels with their much better overall failure record.

Figure 6 describes the wide range of fracture critical cracks (FCC) sizes that resulted in fractures causing derailment. Figures 7, 8, and 9 present the statistical distribution of measured crack sizes, for the failures analyzed by the Union Pacific.

An important aspect of the frequency distribution of FCC sizes is that the highest fracture frequency is developed for crack sizes in order of 0.75 inches. This is the surface length, dimension (C). The smallest crack size for failure is in the order of 0.4 inches (C). The largest crack sizes are in the order of 1.5 to 2.5 inches (C). There is a low frequency for development of fractures due to cracks of small and large (C) dimensions.

A plot of the frequency distribution curve for the FCC sizes is presented at the bottom of Figures 7, 8, and 9. The significance of the peak frequency crack sizes is discussed in the following section.

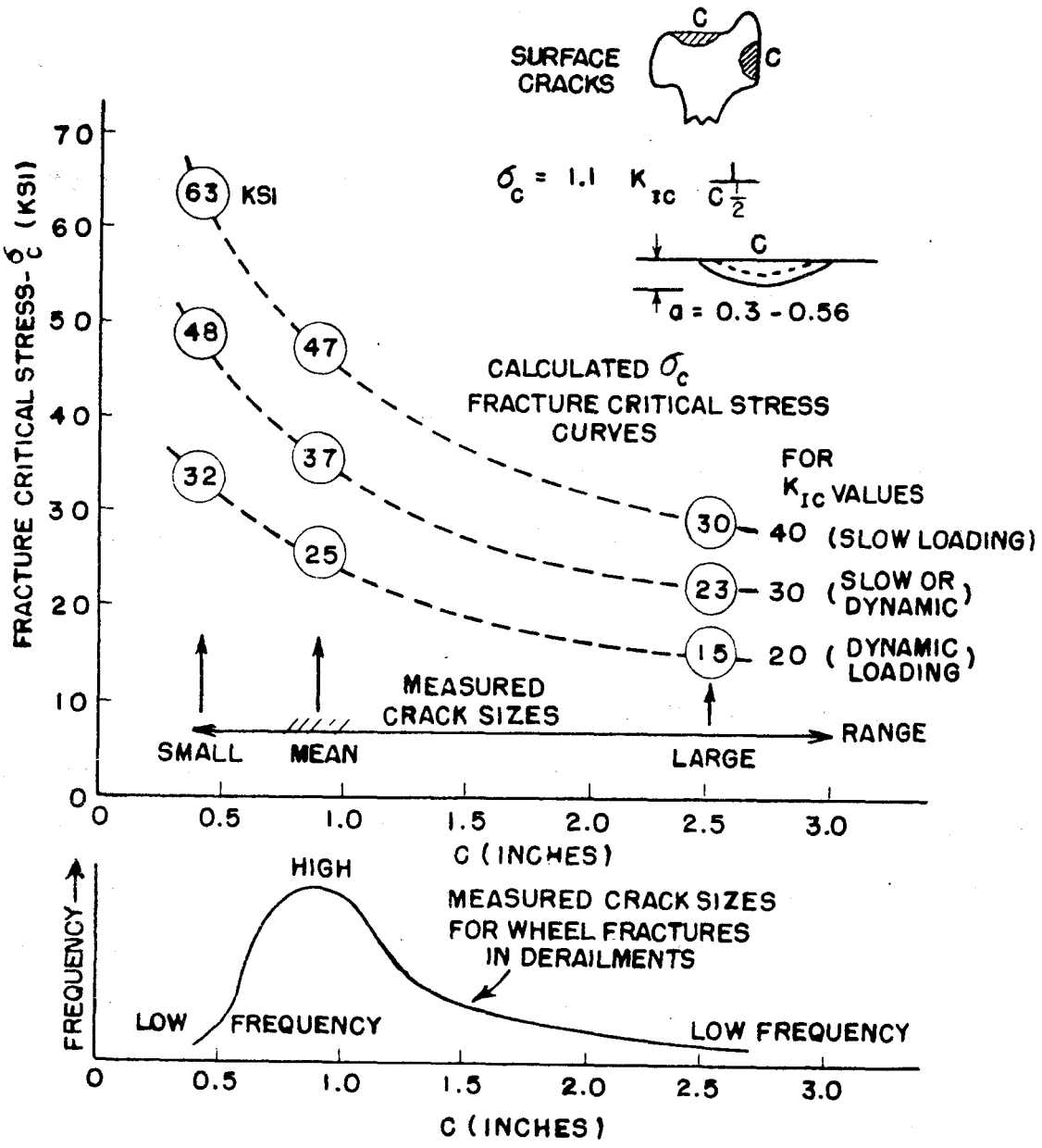

FIGURE 7 FRACTURE STRESS -VS- CRITICAL CRACK SIZE FOR SURFACE CRACKS

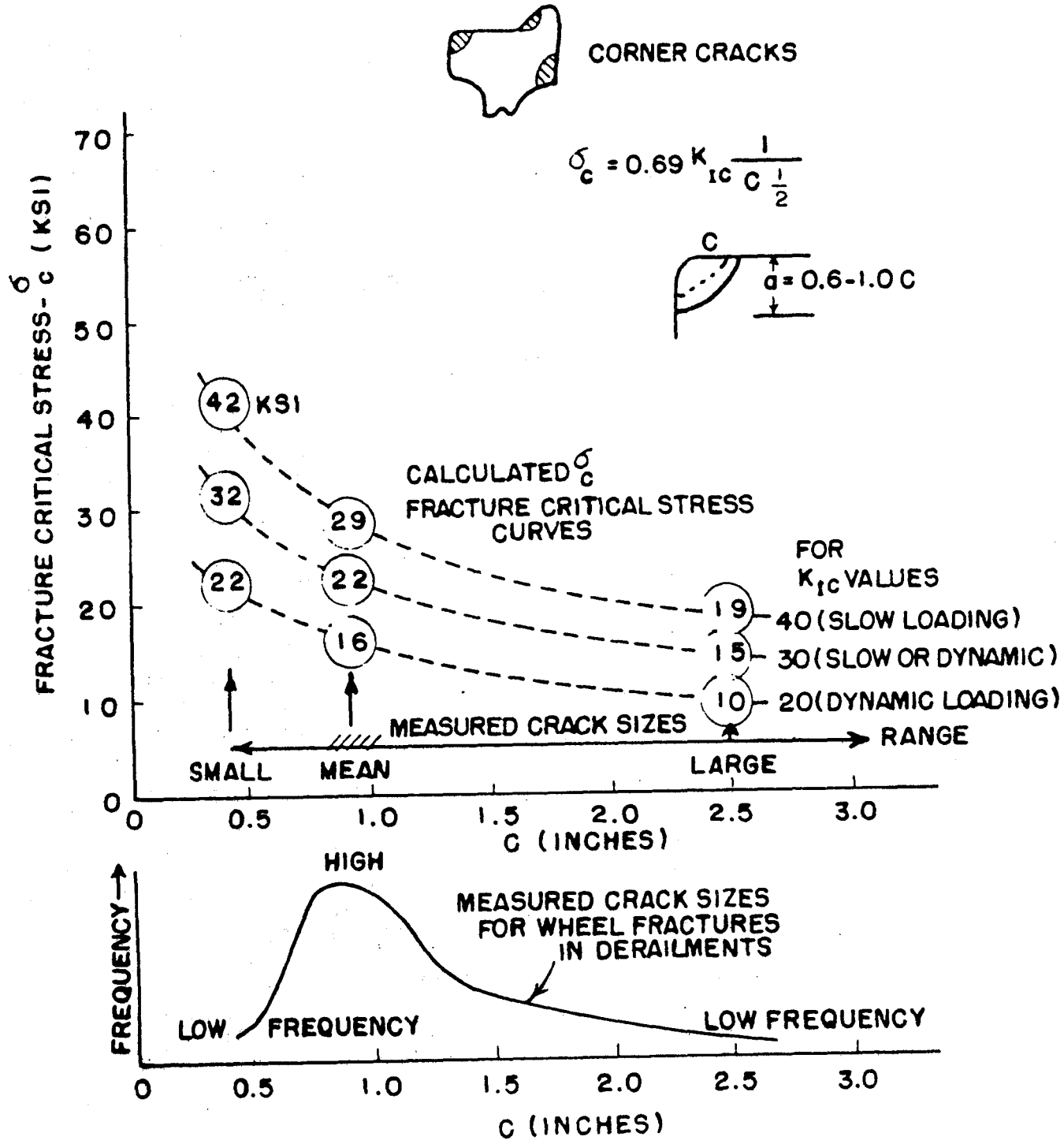

FIGURE 8 FRACTURE STRESS -VS- CRITICAL CRACK SIZE FOR CORNER CRACKS

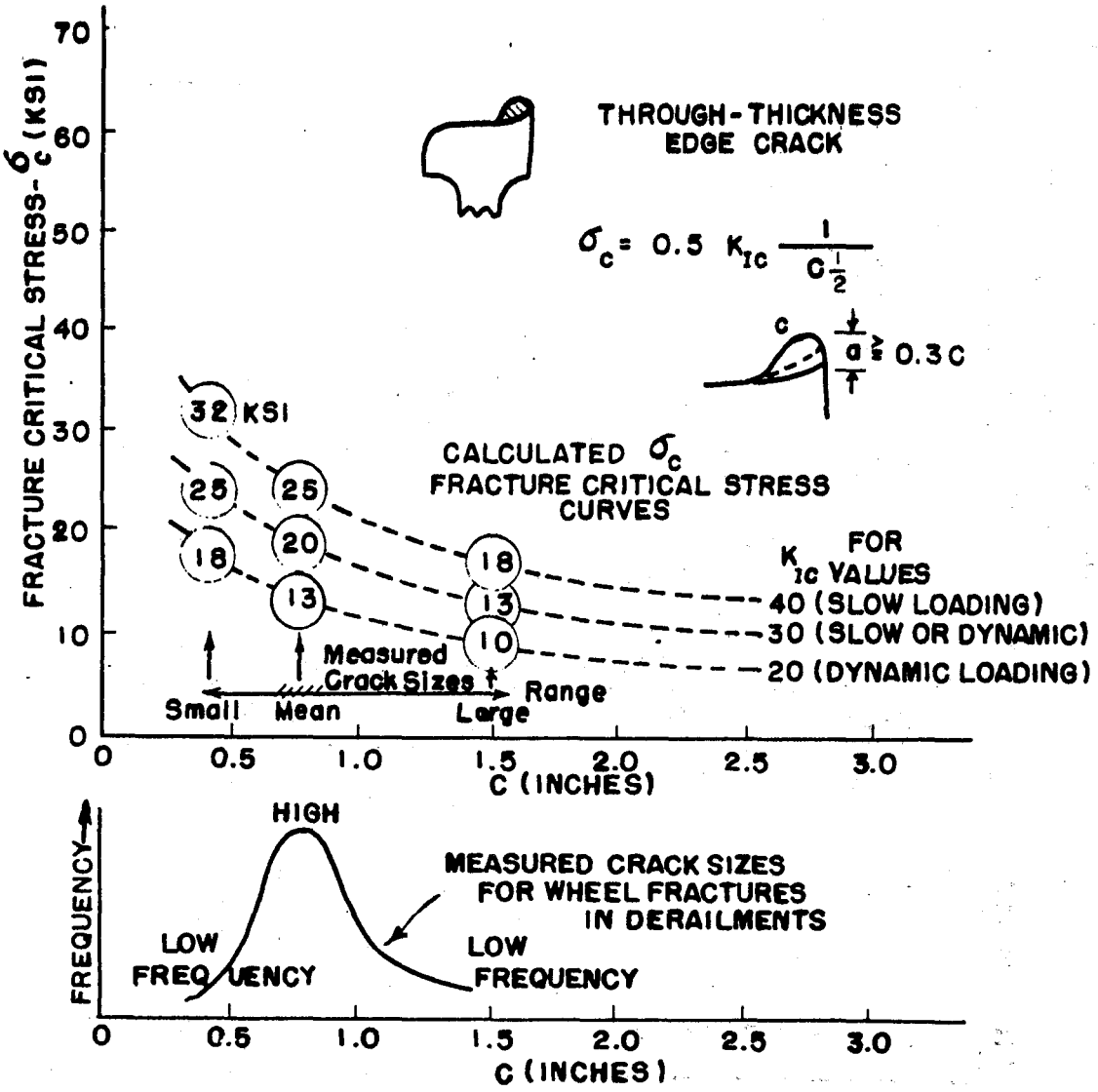

FIGURE 9 FRACTURE STRESS -VS- CRITICAL CRACK SIZE FOR THROUGH-THICKNESS EDGE CRACKS

A summary of K_{Ic} (ksi$\sqrt{in}$) fracture properties for cast and wrought B, C, and U wheels is presented in Figure 10. Because of similar microstructure and strength levels, the K_{Ic} values fall in a narrow range.[3] The lowest values are developed for the case of dynamic (impact) loading rates. These K_{Ic} values are representative of highly brittle steels. This very low level of steel fracture properties has been accepted because of the need for high wear resistance.

The reproducibility of the data from the K_{Ic} fracture tests is in the order of ± 5 ksi$\sqrt{in}$. The lowest value that is feasible to measure is approximately 20 ksi$\sqrt{in}$. The envelope as defined in Figure 10 provides the best description for the fracture properties of any wheel.

Characterization of K_{Ic} values for each wheel involved in a derailment fracture is not practical because it is very expensive and would almost certainly yield K_{Ic} values that fall in the envelope.

The K_{Ic} values are of primary interest for calculation of the fracture critical stress (FCS) for cases of specific measured crack sizes. For this purpose, the calculations may be made using the Reference K_{Ic} values cited in Figure 9. The highest value of 40 ksi$\sqrt{in}$ is for the case of slow loading. The medium value of 30 ksi$\sqrt{in}$ is considered to be a representative value.

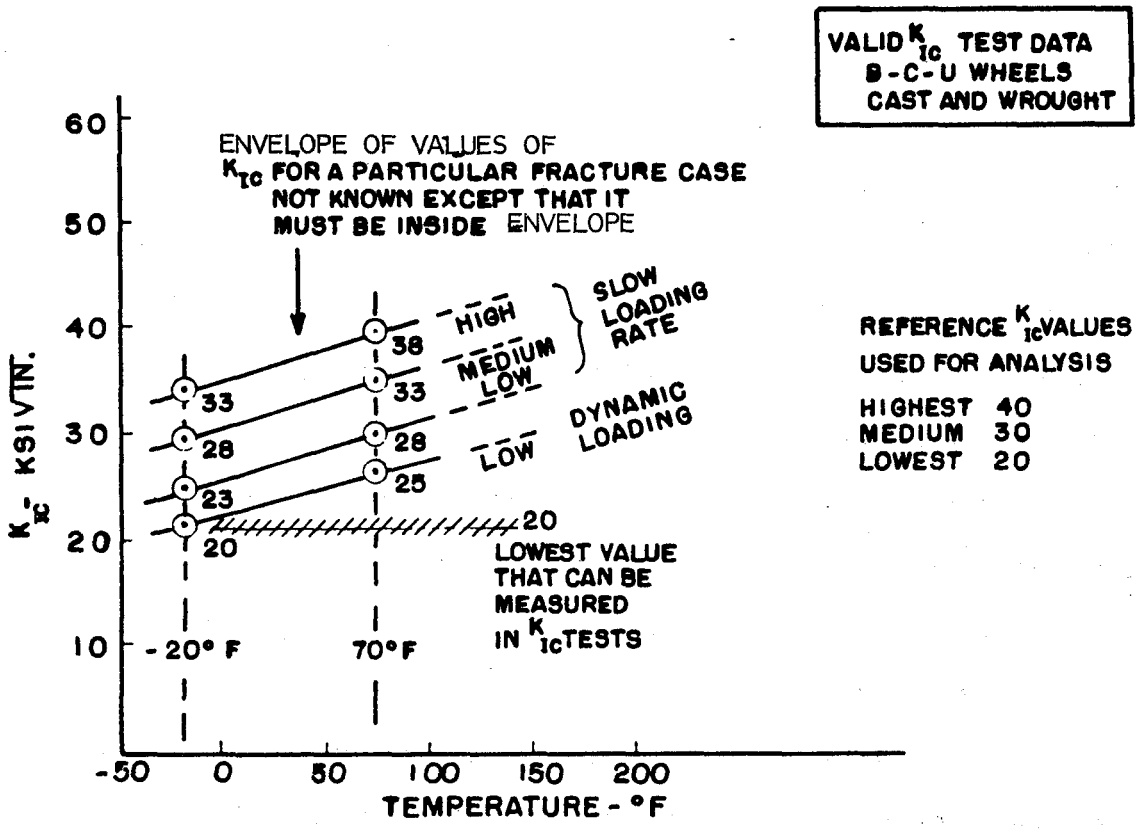

FIGURE 10 EXTREMES OF FRACTURE TOUGHNESS VALUE REPORTED OVER THE TEMPERATURE RANGE OF -20^{O}F TO 70^{O}F (-29^{O}C TO 21^{O})

2.2.1 Fracture Crack Arrest and Fatigue Tests

The crack arrest fracture toughness (K_{Ia}) properties of Class U and C wheel steels were examined. Notched test specimens, taken from the rim portion of appropriate wheels, were wedge-loaded until rapid crack extension occurred. A complete description of test conditions, results, and conclusions appears in Appendix 4.2. The results of this study indicate that the crack arrest fracture toughness of heat-treated Class C wheel steel, is somewhat higher than untreated Class U steel at room temperature, and that this difference increases with temperature (Figure 11).

A dependency of K_{Ia} values on test temperature was noted for Class C steel, while Class U steel appeared fairly insensitive to temperature. This difference appears to be related to the effect of interlamellar pearlite spacing on crack propagation in the steel.

Based solely on the K_{Ia} data, it may also be concluded that rim heat-treated wheels could arrest larger thermal cracks, prior to unstable propagation, than untreated wheels. The critical flaw size tolerated would increase with temperature for the Class C wheels. This behavior would not appear in Class U wheels which are tested below 200^{o}F.

A comparison of actual wheel failure data revealing critical flaw size prior to full failure showed fairly good agreement for Class U data, but suggested that predictions for critical flaw size tolerance for the Class C wheels based on K_{Ia} values were too large.

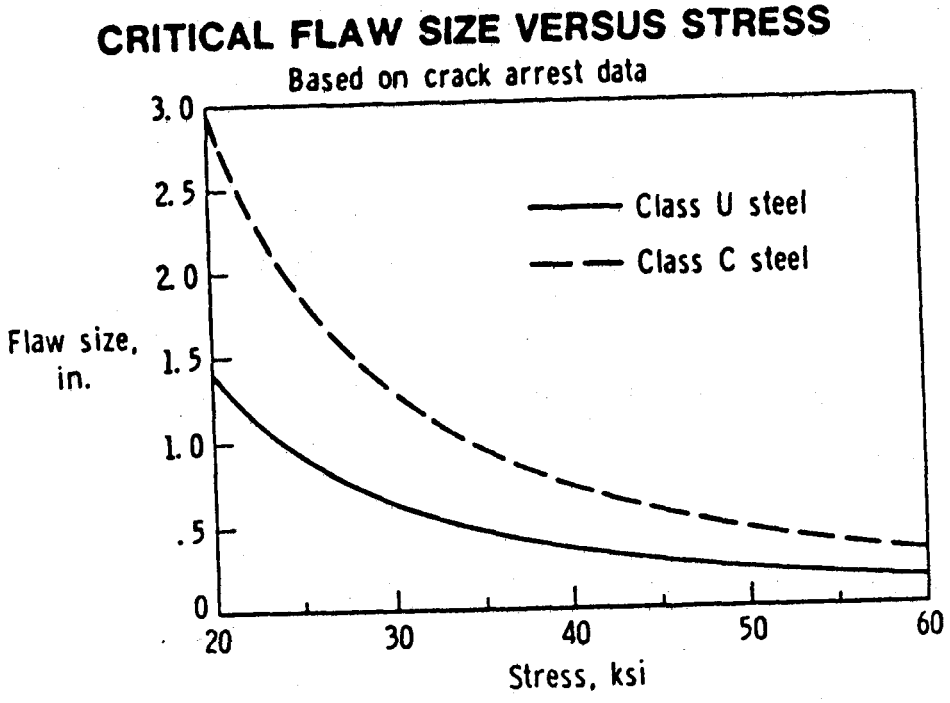

FIGURE 11 CRITICAL FLAW SIZE -VS- STRESS FOR WHEEL STEELS, BASED ON CRACK ARREST DATA

Fatigue life properties of railroad wheel steels have never been determined. A program investigating high temperature fatigue properties of these materials has been completed at the Association of American Railroads. A high temperature testing facility was developed to monitor these tests and determine these properties. Through low cycle fatigue testing, more accurate predictions of fatigue lives of heel steels can be made. Three different grades of wheel steels, B, C and U were used for analysis. These steels were tested at room temperature, 200, 400 and 600°.

2.2.2 Results

The cyclic fatigue properties derived from these tests are listed in Table 2.

TABLE 2

FATIGUE PROPERTIES FOR
CLASSES B, C AND U WHEEL STEEL

Wheel Steel	Temp. C	$\sigma f'$ (ksi)	b	ef'	c	K' (ksi)	n'
B	25	224	-0.106	0.631	-0.606	243	0.175
B	200	303	-0.156	0.257	-0.595	433	0.263
B	400	196	-0.114	2.590	-0.879	174	0.130
B	600	76	-0.093	0.918	-0.739	77	0.125
C	25	260	-0.111	1.850	-0.721	237	0.154
C	200	222	-0.092	0.147	-0.468	324	0.196
C	400	187	-0.096	8.700	-0.982	152	0.098
C	600	68	-0.075	1.921	-0.828	64	0.091
U	25	180	-0.101	0.528	-0.587	201	0.172
U	200	159	-0.102	0.147	-0.448	246	0.228
U	400	166	-0.118	1.685	-0.771	153	0.153
U	600	81	-0.104	0.762	-0.698	84	0.148

$\sigma f'$ -- Fatigue strength coefficient
b -- Fatigue strength exponent
e_f' -- Fatigue ductility coefficient
c -- Fatigue ductility exponent
K' -- Cyclic strength coefficient
n' -- Cyclic strain hardening exponent
(1 ksi = 6.8948 MPA)

The cyclic stress-strain relationship can be expressed by an equation of the following form:

$$\sigma/2 = K' \ (e_p/2)^{n'}$$

The strain-life and stress-life curves are described by the equations:

$$e/2 = (\sigma_f'/E) \ (2N_f)^b + e_f' \ (2N_f)^c$$

$$\sigma/2 = \sigma_f' \ (2N_f)^b$$

The heat treated wheel materials (C and B) exhibit a higher resistance to fatigue than the unheat-treated U wheel material. The higher carbon C material shows better resistance to fatigue than the lower carbon B material. It is clear that the differences in material performance are more pronounced at longer lives (low strain amplitudes) than at shorter lives (high strain amplitudes).

2.2.3 Thermal Cracking Test

The purpose of these tests was to develop a laboratory technique to produce thermal cracking in wheels and to evaluate the relative resistance to such cracking of Class B, C, and U wheels. The mechanism for the cracking being studied is the restrained contraction of untempered martensite, which is similar to the mechanism of quench cracking.

To produce this condition, a localized portion of the wheel tread is heated to a temperature exceeding 1333^{o}F to obtain some transformation to austenite. Then this localized region is cooled fast enough for the austenite to transform to martensite. The restraint provided by the unheated remainder of the wheel during subsequent cooling should produce sufficiently high stresses to crack the brittle martensitic region. An apparatus was constructed and runs were conducted with instrumented wheels.

2.2.4 Apparatus

To enforce the above conditions, a machine (lazy susan) was constructed to support the wheel in a vertical position by the bore and to turn it at speeds of 1 rpm and slower. Further, an oxygen-acetylene burner was supported and clamped so that the distance from the torch tip could be adjusted. A steel pan, measuring 10 inches wide by 48 inches long by 11 inches deep, was fitted with a standpipe and drain, placed beneath the wheel,

so that the lower 9 inches of the wheel was submerged in water. The make up water was provided by two low pressure nozzles directed at the wheel plate, about 12 inches above the water level in the pan.

The wheel was fitted with eight 1/16 inch diameter sheathed thermocouples in holes, drilled to the mid-tread positions from the back face of the rim. The 1/8 inch diameter holes were centered 1/4", 1/2", and 1" from the tread. After the thermocouples were placed in the holes, steel wool was packed around the thermocouples. The thermocouple data were acquired by a modified personal computer for data acquisition, storage, and printout.

All of the wheels for these tests were CJ33 with a parabolic plate. Four Class B, four Class C, and five Class U wheels were designated for these tests. One of the Class U wheels was drilled for the placement of thermocouples in the rim. This wheel was used for development of the test procedure.

As Figures 12 and 13 clearly show, there is no significant difference between the different classes of wheels with regard to when they will crack. At both temperatures, the wheels cracked at about the same number of revolutions.

An explanation for the lack of difference between the different classes of wheels can be found in work by Fec and Sehitoglu[12]. They used hourglass-shaped specimens made out of Class U wheel material. These specimens were rigidly held at each end in water-cooled grips, while the center was cyclically heated by an induction heater until the specimen cracked. The

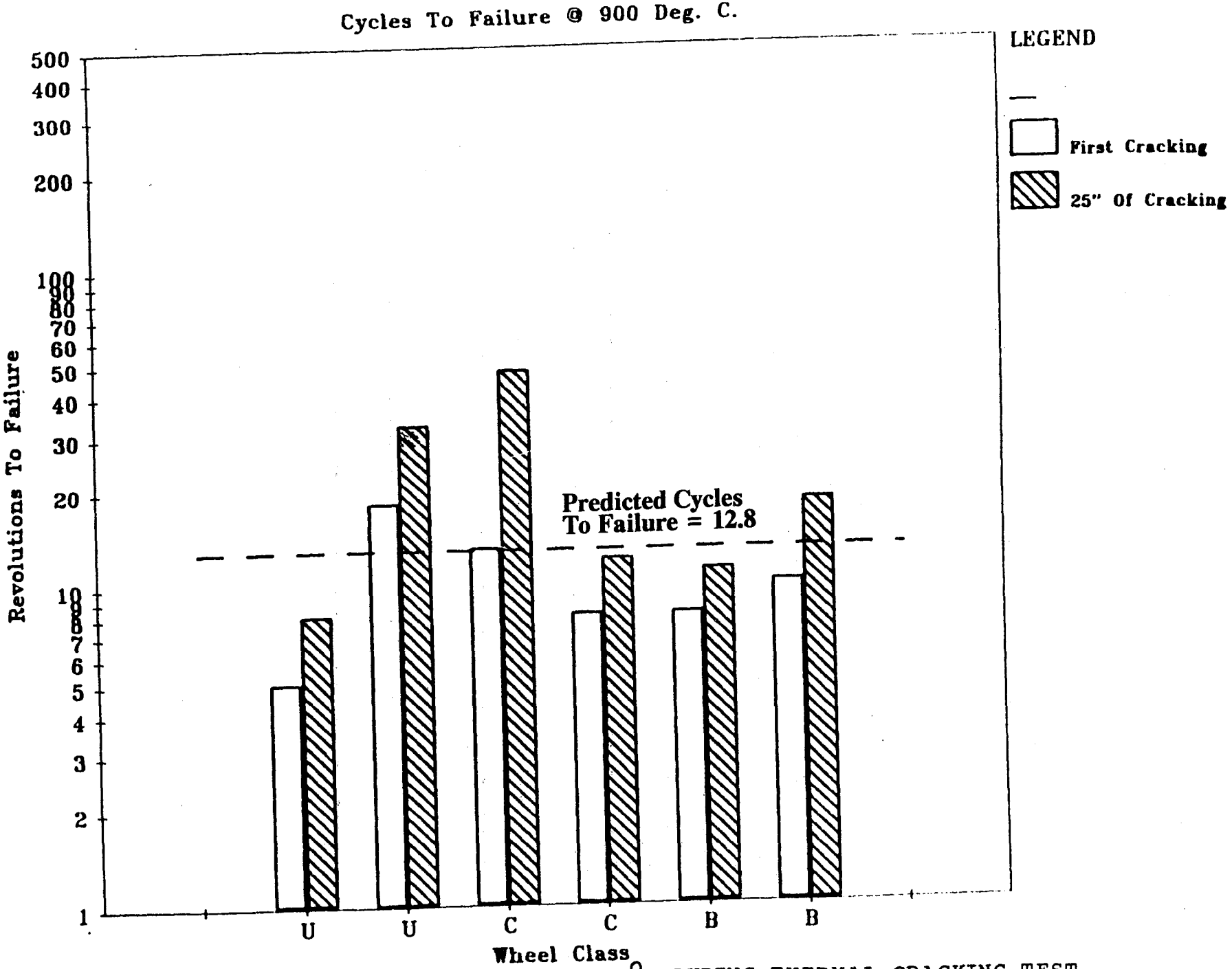

FIGURE 12 REVOLUTIONS TO FAILURE AT 900°C DURING THERMAL CRACKING TEST

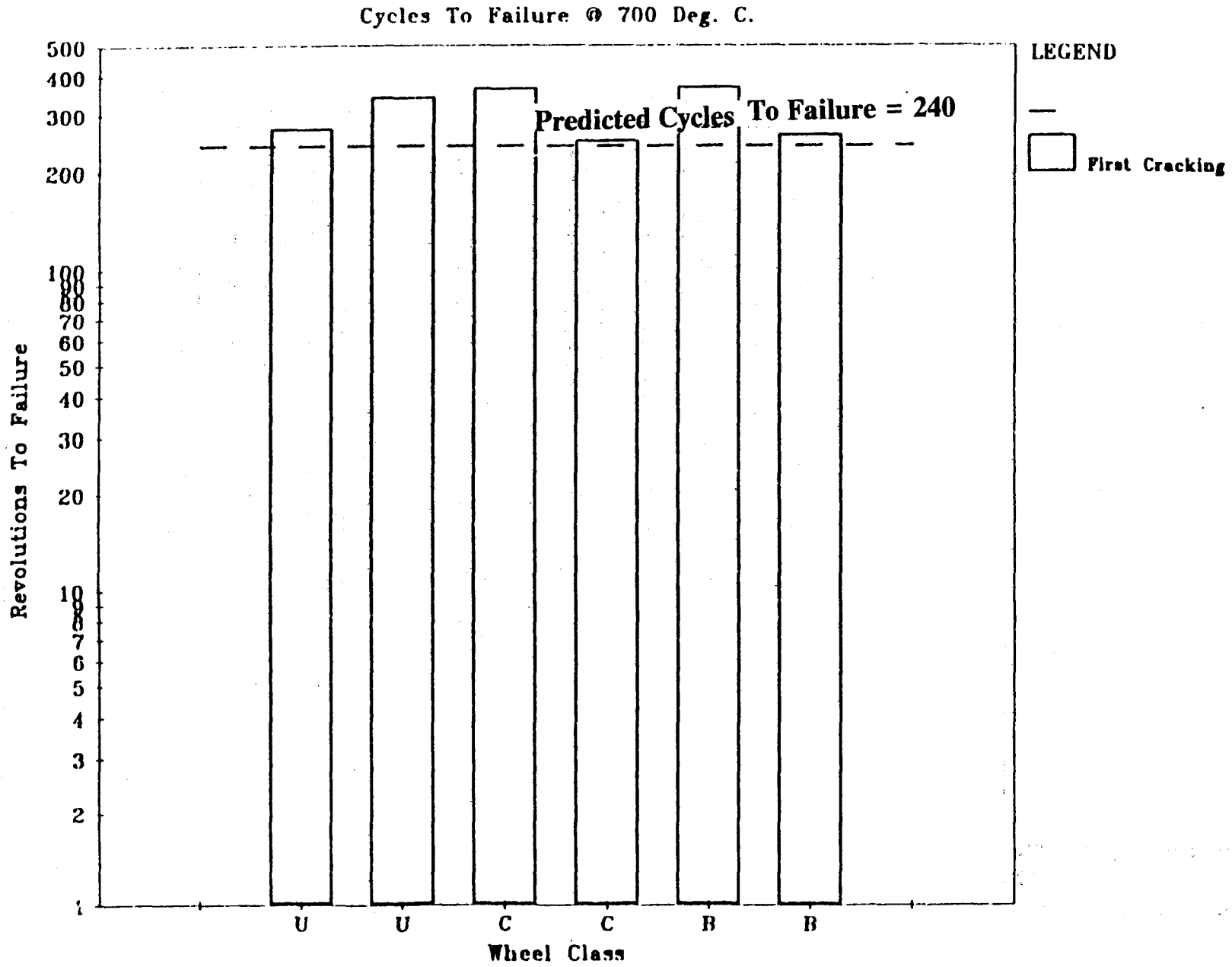

FIGURE 13 REVOLUTIONS TO FAILURE AT 700^{O}C DURING THERMAL CRACKING TEST

net strain from such cycling is 0, as shown in the equation.

$$e_{th} + e_m = 0 \qquad [1]$$

where e_{th} is the thermal strain and e_m is the mechanical strain. Then,

$$\Delta e_{th} + \Delta e_m = 0 \qquad [2]$$

The thermal strain is defined as:

$$\Delta e_{th} = \alpha \Delta T \qquad [3]$$

where α is the thermal expansion coefficient and ΔT is the difference between maximum and minimum temperatures of the thermal cycle.

The mechanical strain can be defined by the Coffin-Manson Law:

$$\Delta e_m = a N_f^{-b} \qquad [4]$$

a and b are constants, while N_f is the number of cycles for cracking to occur.

Fec and Sehitoglu determined that the value of a is 0.01595 and b is 0.1148. α was measured to be 0.000017/^{o}C. For plain carbon wheel steels, this value of the thermal expansion coefficient changes insignificantly between the different wheel

classes.

By substituting Equations 3 and 4 into Equation 2 and rearranging, Fec and Sehitoglu defined the cycles to failure as:

$$N_f = (0.000017(\Delta T)/0.01595)^{(-1/.1148)} \quad [5]$$

Figure 14 shows a plot of the results of this equation, cycles to failure versus ΔT.

To apply Equation 5 to the lazy susan results, ΔT has first to be determined. The minimum temperature in the cycle is 38°C. If the maximum temperature in the cycle is assumed to be the temperature of the hot spot, then for the 900°C test, T would be 862°C. However, the maximum temperature is really a gradient which involves the cooler material surrounding the hot spot. Thus, an effective ΔT has to be established. Based on the thermocouple data taken from the rim region, it was established that for a hot spot temperature of 900°C, the effective ΔT is 700°C.

At a hot spot temperature of 700°C, the effective ΔT is 500°C. Then, at a surface temperature of 900°C, the expected number of revolutions to failure is 12.8 while for a surface temperature of 700°C, the predicted number of revolutions to failure is 240. These predicted values have been plotted on the graphs in Figures 12 and 13.

The predicted number of cycles to failure agrees well with the number of cycles before first cracking is observed in the wheel, particularly at 900°C. At 700°C, note that the

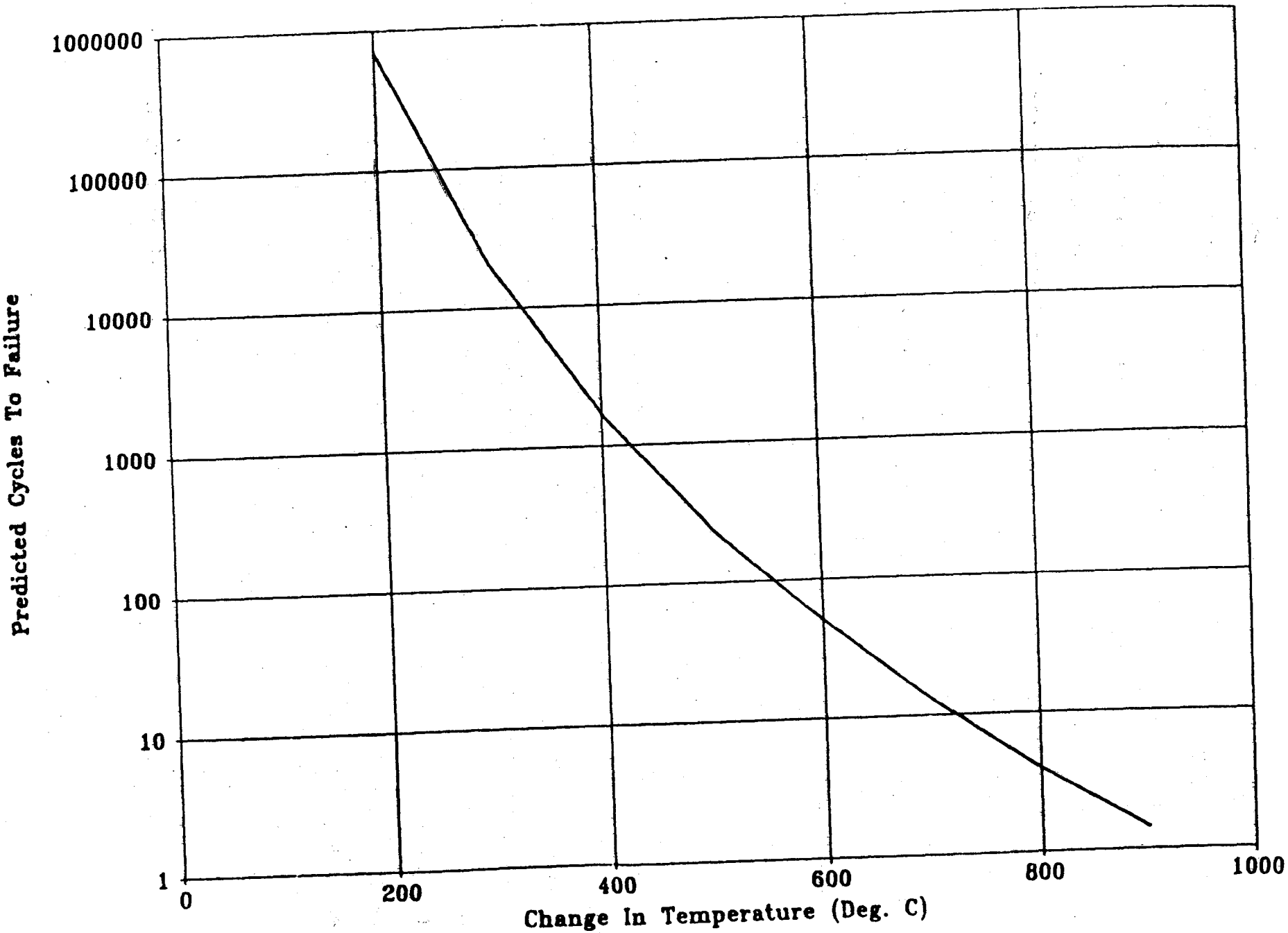

FIGURE 14 CYCLES TO FAILURE -VS- CHANGE IN TEMPERATURE FOR B, C AND U WHEELS

number of cycles for first cracking to occur was higher than predicted in all cases. The reason for this is that the liquid penetrant was not sensitive enough to pick up initial cracking. Near the end of testing, a new magnetic particle tester was subsequently obtained to detect cracking. This unit found cracks 50 to 60 revolutions before the dye penetrant did on the two wheels it was used on. It is felt that at 700°C, the results would be closer to the predicted values, if this magnetic particle detector had been used. (For the sake of comparison, none of the results reported at 700°C were based on the magnetic particle detector). Rather, results were reported based on the dye penetrant test.

2.2.5 Conclusions

Based on the thermal cycling testing performed, there is not any significant difference in performance between the Class B, Class C, and Class U wheels in regard to when they will first crack. It should be noted that in the case of wheel crack initiation, this process is "short circuited" by the production of stress risers because of the occurrence of wear. Rather, cracking can be predicted by the empirical model developed by Fec and Sehitoglu [1]:

$$N_f = (\alpha \Delta T / 0.01595)^{(-1/0.1148)}$$

The only part of this equation based on material properties

is the thermal expansion coefficient, α , which varies little between the three classes of wheels. Here it was assumed to be a value of 0.000017/^{o}C.

Based on both the logic behind the model and the agreement of the lazy susan experimental results with it, it is felt that the Fec and Sehitoglu model can adequately predict the number of cycles to failure, in this situation.

2.3 General Observations Regarding Failure

From this investigation of wheel failures from the information obtained from selected railroads, the following conclusions can be drawn:

1. Small cracks do not cause frequent fracture because of the infrequent application of high crack-opening stresses.
2. Therefore, the small cracks grow until their size is sufficiently large to result in fracture for the more frequently applied levels of crack-opening stresses.
3. Only a few cracks grow to larger sizes which can then fail due to low levels of applied crack-opening stresses.

The prior section indicated that medium size cracks were most frequently responsible for fracture initiation. This observation is supported by the actual measurement of crack

sizes for the case of fractures resulting in derailments.

The calculations of fracture critical stresses (FCS) were based on K_{Ic} fracture properties involving a narrow range of K_{Ic} values. Because of this narrow range, one set of properties can be considered to apply to wheels of B, C, and U types. The possible differences due to loading rate are very small and are not statistically of major significance.

It follows that the most frequent cause of fracture initiation is the combination of medium size cracks and medium level crack-opening stresses. In order to understand the process of failure, several factors must be considered.

One critical factor is the spectrum of residual tensile stresses that are developed in the rim circumference of the wheels. Cracks grow in size as a result of repeated application of mechanical load and thermal stresses. The growth rate is determined by the stress level and the cyclic frequency.

Another critical factor is the peak stress, since fracture occurs at the application of a stress when the stress is sufficiently high to cause rapid growth of the crack. Therefore, stress peaks in the spectrum of service stresses are a critical factor. The stress peaks represent short pulse events in which normal low levels of repeated applied stresses are exceeded. There are numerous reasons for the development of stress peaks which are superimposed on the spectrum of normal (low) stress cycling. These include wheel impact at joints or switches, truck hunting, car rocking, and tread irregularities.

The stress peaks of interest are circumferentially applied

tensile stresses which act to open rim or flange cracks. A small part of the wheel circumference is affected by a single stress peak. This is due to the very short time of the stress peaks. This pulse acts only on a small part of the circumference. In failure analysis reports, it is often reported that numerous cracks of the same type and size are present. However, if one crack happens to be at the right place, a pulse can cause it to initiate fracture.

2.4 Observations from Field Experience

1. A straight plate wheel is several times more likely to fail and cause a derailment than a curved plate wheel.
2. During a typical year, approximately one half of the derailments occur during the winter quarter.
3. It is impossible from the service data to conclude if there is any difference in performance between U and B or C wheels due to the lack of data available on population or mileage of heat-treated and non-heat-treated wheels.
4. The number of FRA reportable accidents caused by wheel thermal failure is decreasing at a rate of 0.016 accidents per billion ton miles per year (the number of accidents caused by wheel thermal failures was approximately .043 per billion ton miles in 1985).
5. Accident statistics indicate that 60 percent of accidents caused by wheel thermal failure involve

wheels which are not discolored four inches or more. A survey of 12,000 wheels by one railroad showed that approximately five percent of the wheels were discolored. If this five percent applied to the entire fleet, then any straight plate wheel discolored four inches or more is approximately eight times more likely to fail than any straight plate wheel discolored less than four inches. Service data do not provide sufficient information to determine this ratio by wheel design or class.

6. Examination of over 400 wheels show that thermal cracks that lead to failure are always associated with some type of other mechanical or metallurgical damage.
7. Virtually all curved plate wheel failures originate at the sharp point formed at the intersection of the front flange wear line and the original flange profile.
8. The highest probability for the occurrence of a wheel fracture is found when a crack of medium size (3/4-inch) is combined with a medium level combination of residual and service stress (20 to 35 Ksi).

3.0 EXPERIMENTAL PROGRAM

3.1 Saw Cutting

In order for a wheel to fail, two conditions must be present: a crack of sufficient size and a stress of sufficient magnitude to trigger a sudden fracture. This stress is a combination of the service induced stresses and any residual stresses present.

Residual tensile stresses in the hoop direction are not present in the rim of a new wheel when it is manufactured.[4] These stresses are created by service conditions involving severe overheating that leads to an expansion of the rim and yielding of the softened steel. Upon cooling, such a wheel contains a residual tensile stress.

In order to estimate the level of residual stress present in wheels of different design, heat-treatment, size, and amount of discoloration, an extensive program of saw-cutting was undertaken, in addition to other methods such as hole drilling, etc.

In this procedure, a given wheel was cut radially from the flange in towards the hub, and resulting flange tip displacements were measured as a function of saw-cut depth.[5]

In addition to the 387 wheels which were saw-cut at the TTC, 188 service wheels were cut in separate research programs by the Norfolk Southern, Union Pacific, and Santa Fe railroads.

Flange displacement data for the 188 wheels were provided by the railroads and was used to augment data collected at the TTC.

The freight car wheels selected for this study included:

1. Wheels taken out of service by visual inspection of wheel discoloration that extended 4 inches (102 mm) from the rim

into the plate region on one side (AAR Why Made Code 89) and those subsequently taken out of service due to discoloration on both sides (there are 123 wheels in this data set),

2. Wheels taken out of service due to thermal cracks (AAR Why Made Code 74),
3. Wheels taken out of service due to reasons other than AAR Why Made Codes 89 and 74, and
4. 26 new wheels.

In addition to the 387 service wheels, 26 wheels from dynamometer testing and 31 wheels from TTC testing were saw-cut at Pueblo.

If a rail car wheel is cut radially, one of three general types of behavior will usually be observed. A new or undamaged Class U wheel will close at the beginning of the cut, as the cut proceeds into the rim. As the cut approaches the bottom of the rim, the wheel begins to open and continues to open as the cut progresses into the plate, as shown in Figure 15. A heat-treated wheel (Class B or C) which is new or undamaged, exhibits a continually closing behavior during the radial saw-cut, as shown in Figure 16. A thermally damaged wheel, on the other hand, develops increasingly tensile residual stresses as the cut proceeds inward, as shown in Figure 17, and the cut opens. A crack located in this area of tensile stress would probably be able to propagate with no possibility of arrest.

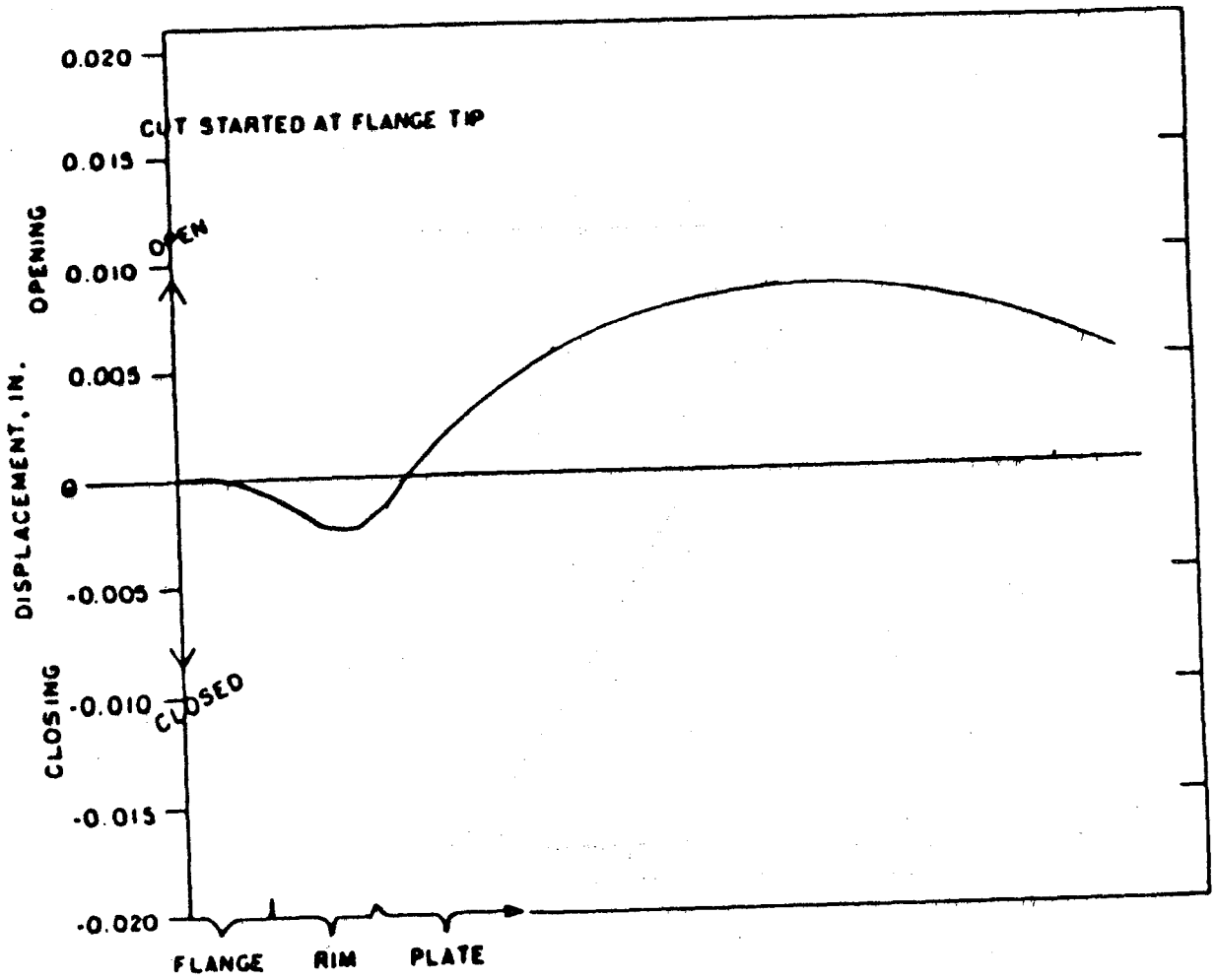

FIGURE 15 TYPICAL SAW-CUT DISPLACEMENT BEHAVIOR OF A NEW OR UNDAMAGED CLASS U WHEEL

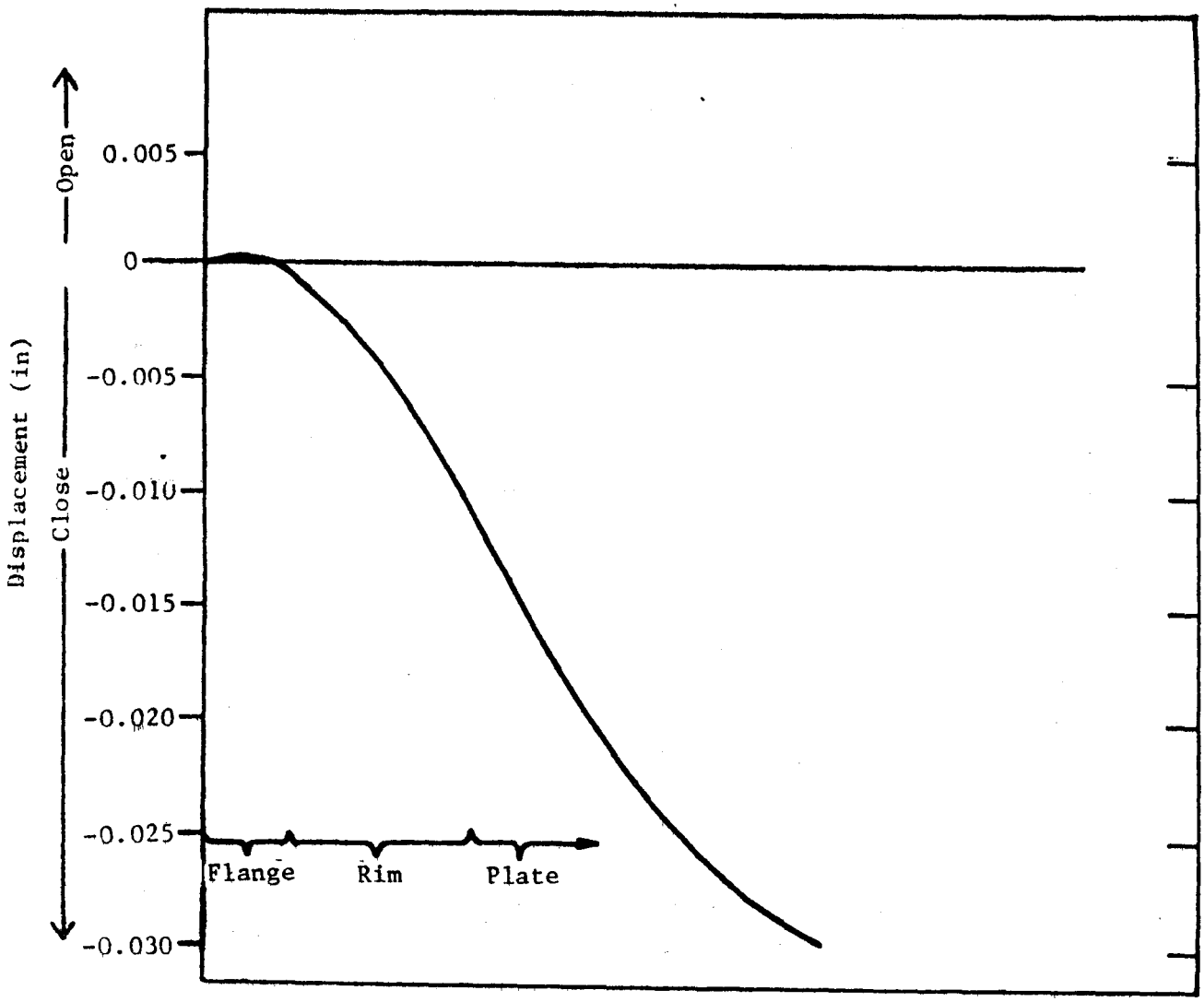

FIGURE 16 TYPICAL SAW-CUT DISPLACEMENT BEHAVIOR OF NEW OR UNDAMAGED CLASS B OR C WHEELS

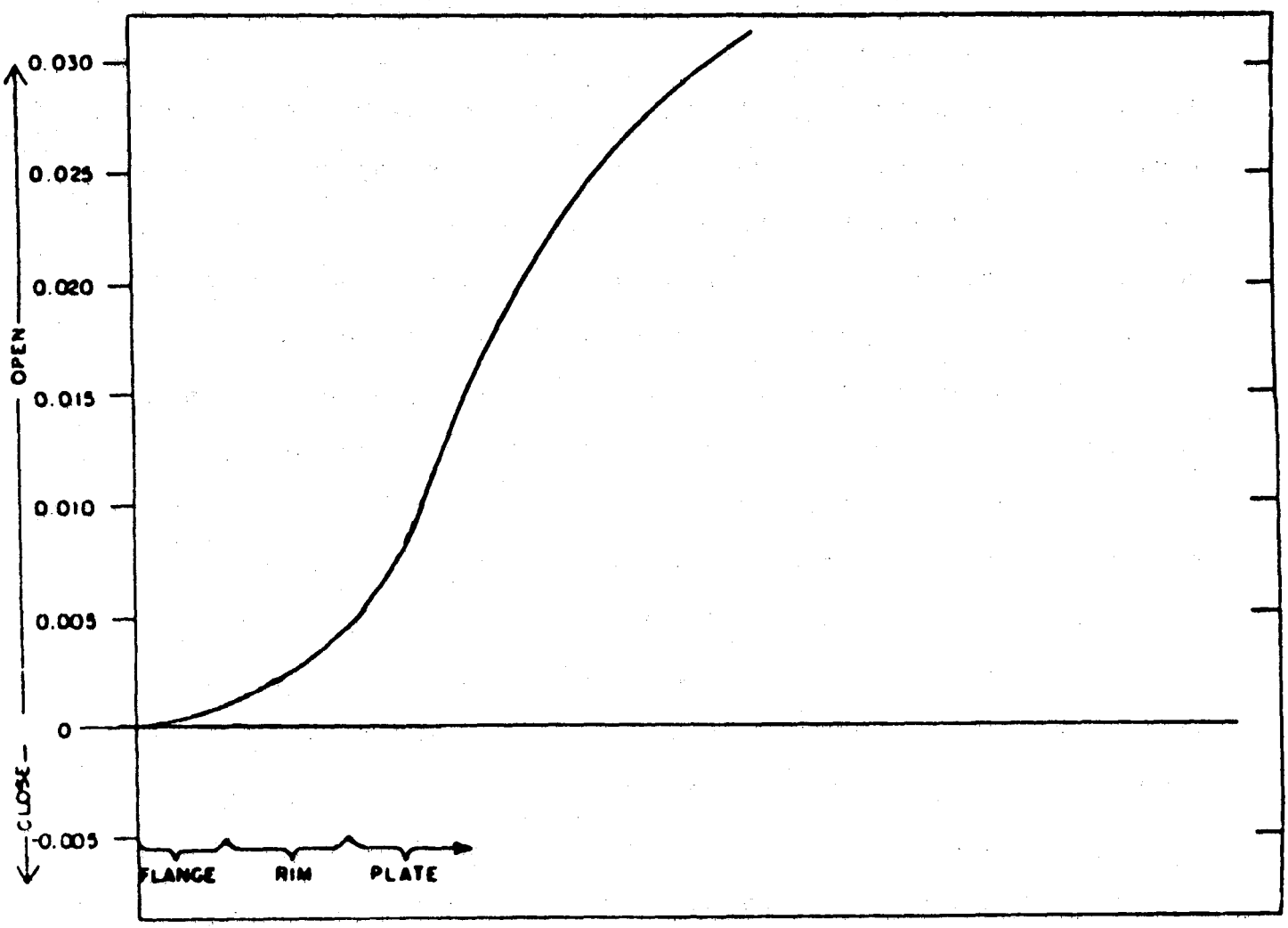

FIGURE 17 TYPICAL SAW-CUT DISPLACEMENT BEHAVIOR OF A THERMALLY DAMAGED WHEEL

3.2 Stress Analysis of Saw Cut Wheels

Two techniques have been developed to translate the saw-cut opening behavior into some measure of rim residual stress. During the implementation of the Wheel Failure Mechanisms Program, two different approaches were taken to evaluate the residual stresses from the saw-cut displacement data. The first approach consisted of measuring the saw-cut opening displacement on both sides of the wheel along the entire length of a cut.[6] A three-dimensional finite element analysis was performed to determine the stresses that result when the first cut is closed. A circumferential displacement loading was assumed on the free surface sufficient to close the cut. The stresses that are calculated for the plane of the cut are then an indication of the stresses that existed before the wheel was cut.

Twenty-eight of the wheels, which were saw-cut under the program, were designated for detailed finite element analysis. These wheels were selected to represent different designs and prior usage. The finite element analysis predicted the residual circumferential stress in the wheel cross section from the flange tip, covering the entire depth of cut. A typical residual stress distribution predicted by this analysis is shown in Figure 18.

The analysis showed a general relationship where the maximum predicted stress in the wheel is a function of the maximum opening of the saw-cut, Figure 19.

The second approach in the evaluation of residual stresses from the saw-cut displacement data consisted of the development of closed form solution for determining the average hoop stress distribution in the saw-cut wheel based on the tip opening behavior.[7]

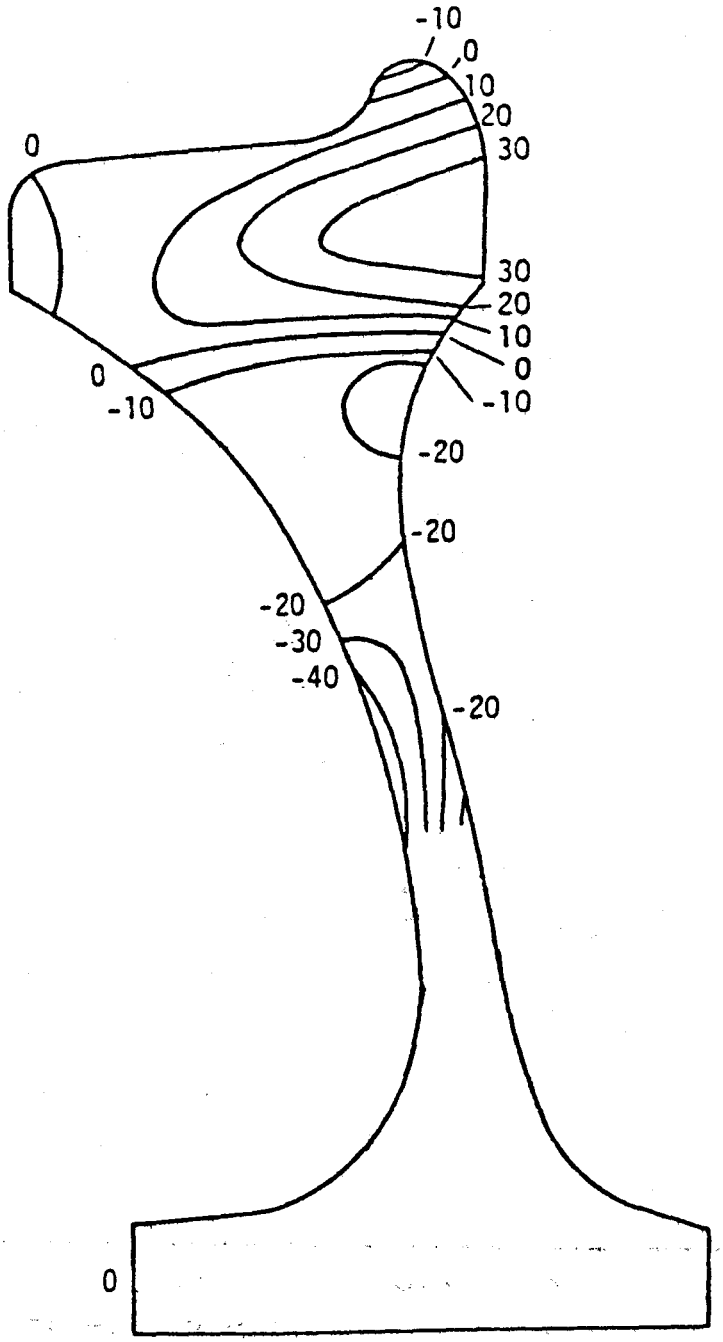

FIGURE 18 RESIDUAL CIRCUMFERENTIAL STRESS DISTRIBUTION PREDICTED FOR 36-INCH DIAMETER CURVED-PLATE WHEEL FROM SAW-CUT DISPLACEMENT DATA (STRESSES IN KSI)

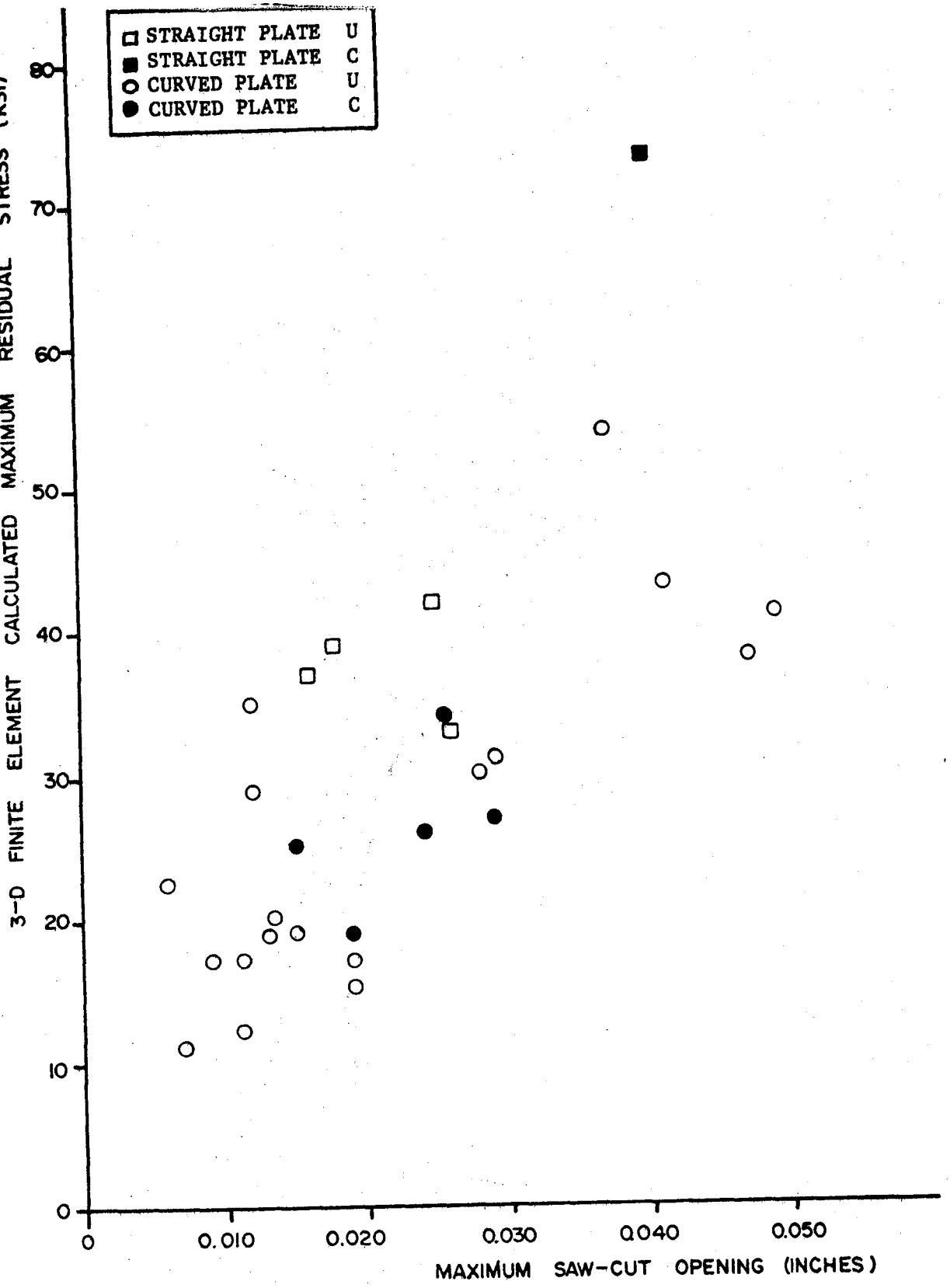

FIGURE 19 MAXIMUM RESIDUAL STRESS CALCULATED BY 3D FINITE ELEMENT ANALYSIS VERSUS MAXIMUM SAW-CUT OPENING

The model assumes that the cut portion of the wheel consists of several interconnected rings. When the radial saw-cut is made, hoop and shear stresses are released on the cut surface, causing individual rings to displace circumferentially and radially. Now, if the cut surfaces are subjected to the released stress distribution, they will merge and the wheel will be in its original position (before the saw-cut). During this process, radial and shear stresses are developed on the interface of adjacent rings, due to relative displacements. The hoop and shear stresses acting on the tip of an individual ring can then be determined as a function of the tip displacement and the stresses on the interface. For this purpose, an individual ring is separated from the rest; and equations based on theory of elasticity are developed for determining stresses acting on the tip, which equilibrate with the stresses on the outer and inner interface, and are compatible with tip displacements. Finally, all the individual rings are reconnected. In the process, the complete hoop and shear stress distribution in the radial direction is generated for the depth of the saw-cut.

In the second approach, the results from the analyses were used to calculate the total circumferential force in the rim of the wheel and this force is suggested as a measure of the fracture potential of the wheel.

The results of 3D-finite element analysis and the second method based on closed form solution were compared for seven wheels. The stress contours from 3-dimensional stress analysis

were integrated over the rim surface and multiplied by the incremental cross section area to determine the effective rim force acting on the rim cross sectional area. These results were surprisingly close as shown in Table 3, with the promise that the second method gives reasonable predictions of rim force, based on the flange tip opening history only.

It is evident from Table 3 that net rim forces computed from saw-cut displacement data using the closed form solution (second method) compare well with the predictions from the 3D-finite element method.

The residual stresses were measured in several of the saw-cut wheels by the hole drilling-strain gaging technique before they were cut. Subsequently, net rim forces were computed for the wheels from their saw-cut displacement data using the closed form solution. The results of the residual stress measurements were compared with the net rim force calculations. Figure 20 shows that a good correlation is found between the net rim force computed from the saw-cut displacement and the surface residual stress on the back rim face as measured by the hole drilling technique.

Figure 20 presents the data for the tests that were carried out for Class U and Class C wheels, tested on the Brake Dynamometer. Each wheel was subjected to 25 drag braking cycles at 40 BHP, each cycle lasting for 45 minutes. From Figure 20, it also can be noted that there is a clear difference in the residual stress state between the heat treated (Class C) wheels and untreated (Class U) wheels for the same level of heat input.

TABLE 3

COMPARISON OF NET RIM FORCE COMPUTED FROM 3-D FINITE ELEMENT ANALYSIS AND 2-D CLOSED FORM ANALYSIS

Wheel No.	Type	Class	Net Rim Force	
			3-D Finite Element Analysis (Kips)	2-D Closed Form Analysis (Kips)
29	CH36	U	+156.5	+152.0
156	CJ33	U	+ 22.5	+ 18.0
30	CH36	U	+163.5	+167.0
72	H36	U	+ 43.2	+ 49.0
21	CH36	U	+ 72.5	+ 69.0
16	CH36	U	+ 15.3	+ 14.0
57	CH36	U	+ 4.6	- 10.0

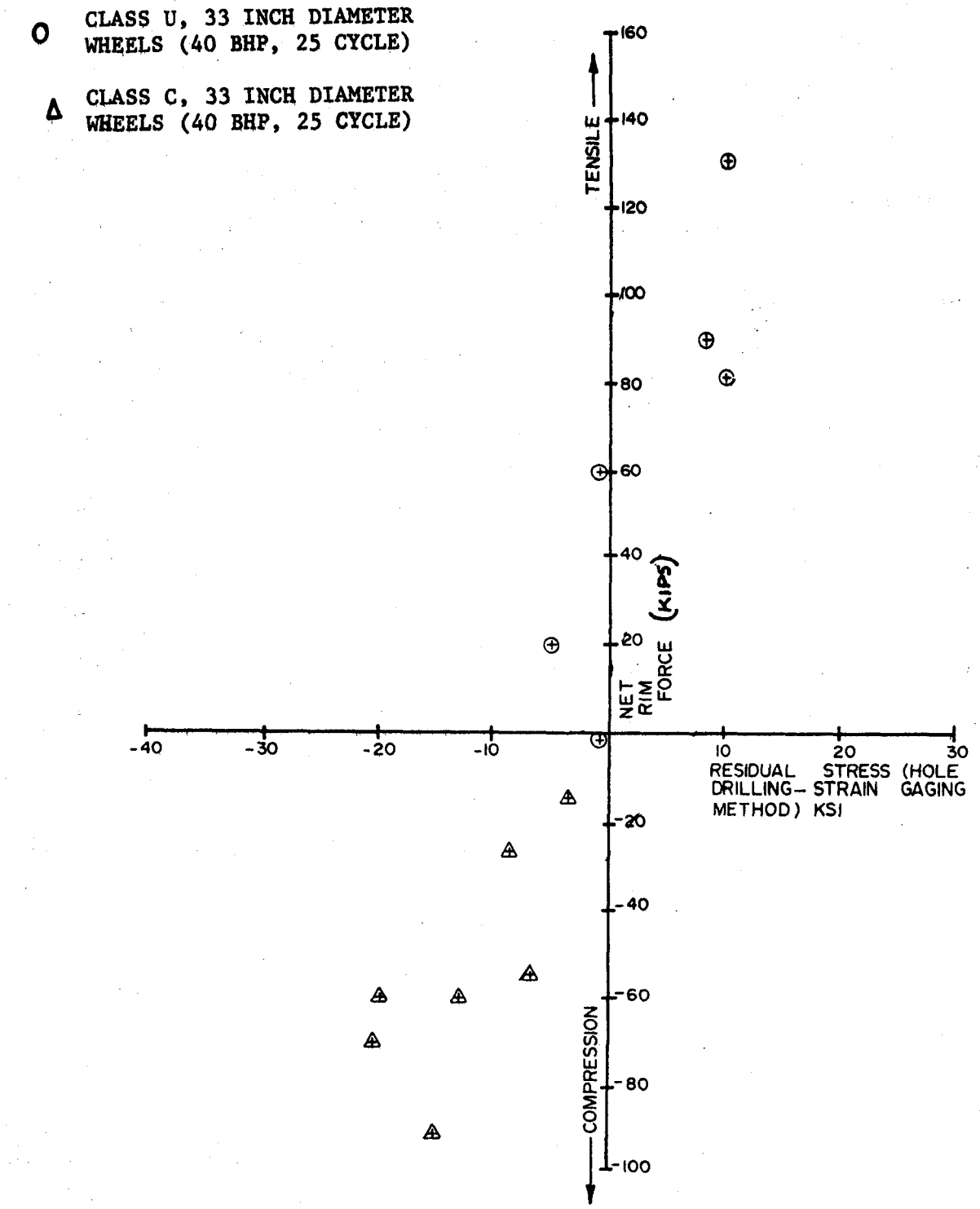

FIGURE 20 RELATIONSHIP BETWEEN NET RIM FORCES (COMPUTED FROM SAW-CUT DISPLACEMENT DATA) AND RESIDUAL STRESS MEASURED ON BACK RIM FACE BY "HOLE DRILLING-STRAIN GAGING" METHOD

From these data, it can be concluded that Class C wheel is much less likely to develop a residual tensile stress in the rim than a Class U wheel.

3.3 Distribution of Residual Stress in the Wheel Population

The distribution of residual stress using the average rim stress index (or net rim force) over the entire population of service wheels that were saw-cut, was investigated.

The closed form analytical model (second method) was used to evaluate the average residual stress distribution (and subsequently the net rim force) for all the wheels that exhibited mixed and opening behavior during saw-cutting. The analysis showed that the majority of wheels that exhibited mixed behavior up to a maximum opening of 0.008 in. had average compressive stresses in the rim. The average residual stress in the rim tended to become tensile above a maximum opening of 0.008 in. (mixed behavior) and the net tensile force varied based on the maximum opening as well as rate of opening.

The results of the 3D-finite element analysis for 28 wheels from the saw-cut displacement data were compared with the results of closed form solution predictions (Figure 21). The 3D-finite element analysis predicts the stress distribution, in the form of stress contours across the wheel cross-section. For the majority of wheels, it was noticed that the maximum circumferential residual stress contour usually originates from the back rim face. This value of residual stress on the back

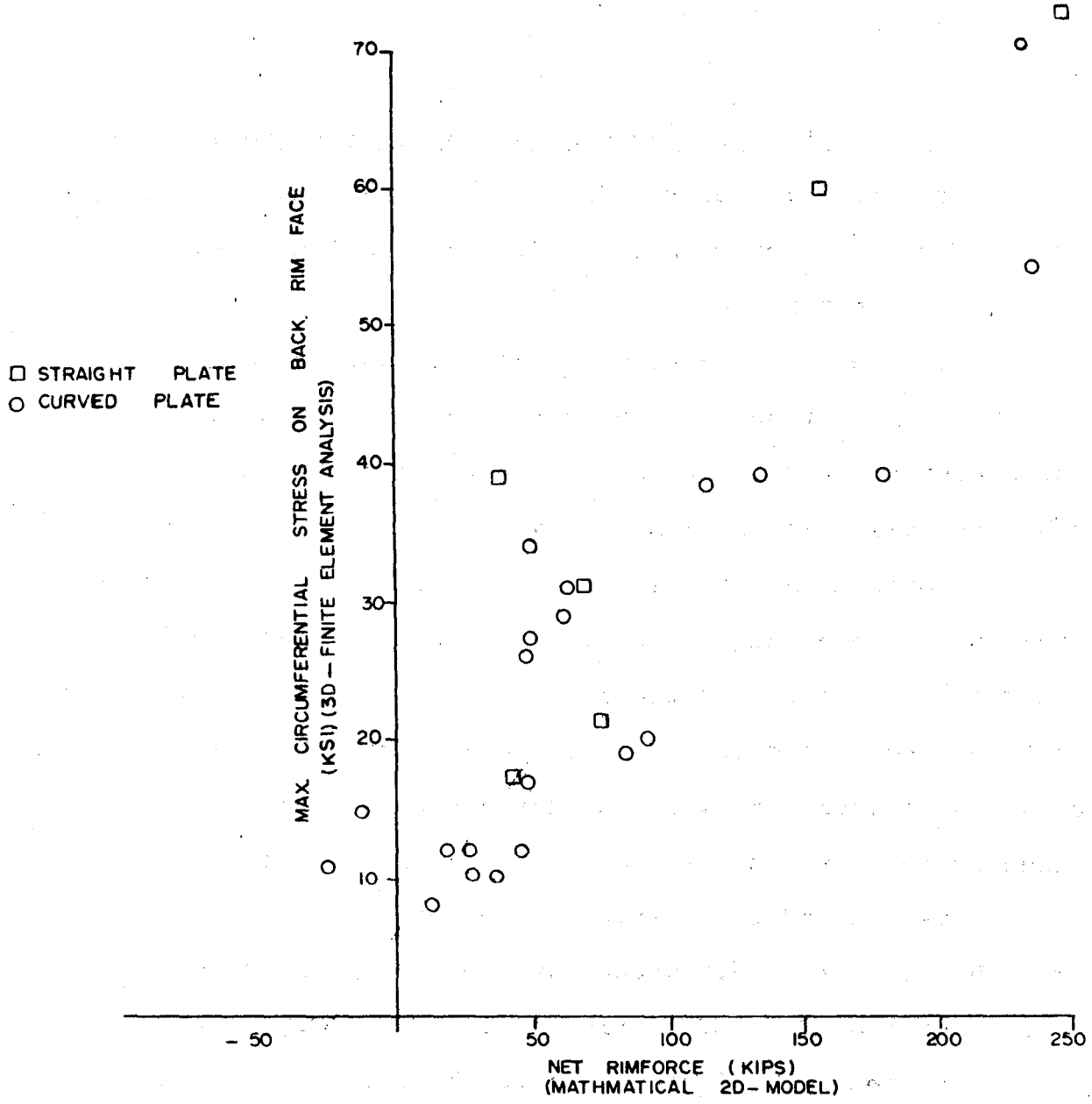

FIGURE 21 MAXIMUM HOOP STRESS ON BACK RIM FACE CALCULATED BY 3D FINITE ELEMENT ANALYSIS VERSUS NET RIM FORCE COMPUTED (BY CLOSED FORM SOLUTION) FROM SAW-CUT DISPLACEMENT DATA

rim face was correlated with the net rim force computed by the second method from the saw-cut displacement data of the same wheel. The maximum circumferential stress on the back rim face (3D analysis) shows a linear relationship with the net rim force computed by the simple analytical model. A net rim force of 100 Kips (8.5 Ksi tensile average) corresponds to the occurrence of a maximum circumferential residual stress of about 25 Ksi on the back rim face. Additionally, 8.5 Ksi is below the level of stress necessary to propagate a fracture (Figures 7, 8, and 9). Based on this comparison, a net rim force (tensile) of 100 Kips can be regarded as the cut-off point to classify wheels of low fracture potential.

Figures 22 and 23 and Table 4 show the saw-cutting data segregated on the above basis for Class U and Class C wheels. These data show that heat-treatment is as effective as design in resisting thermal damage. Heat treatment appears to be more effective in curved plate wheels than in straight plate wheels.

An effective graphical method of presenting distribution information is cumulative probability plotting. Figure 24 presents the cumulative percentage of curved plate wheel population versus the net rim forces computed from the saw-cut displacement data.

Figure 25 presents the similar information for straight plate wheel population that were saw-cut.

As an example of the interpretation of these plots, consider the meaning of the straight line representing the Subgroup of straight plate, Class U, discolored wheels from Figure 25.

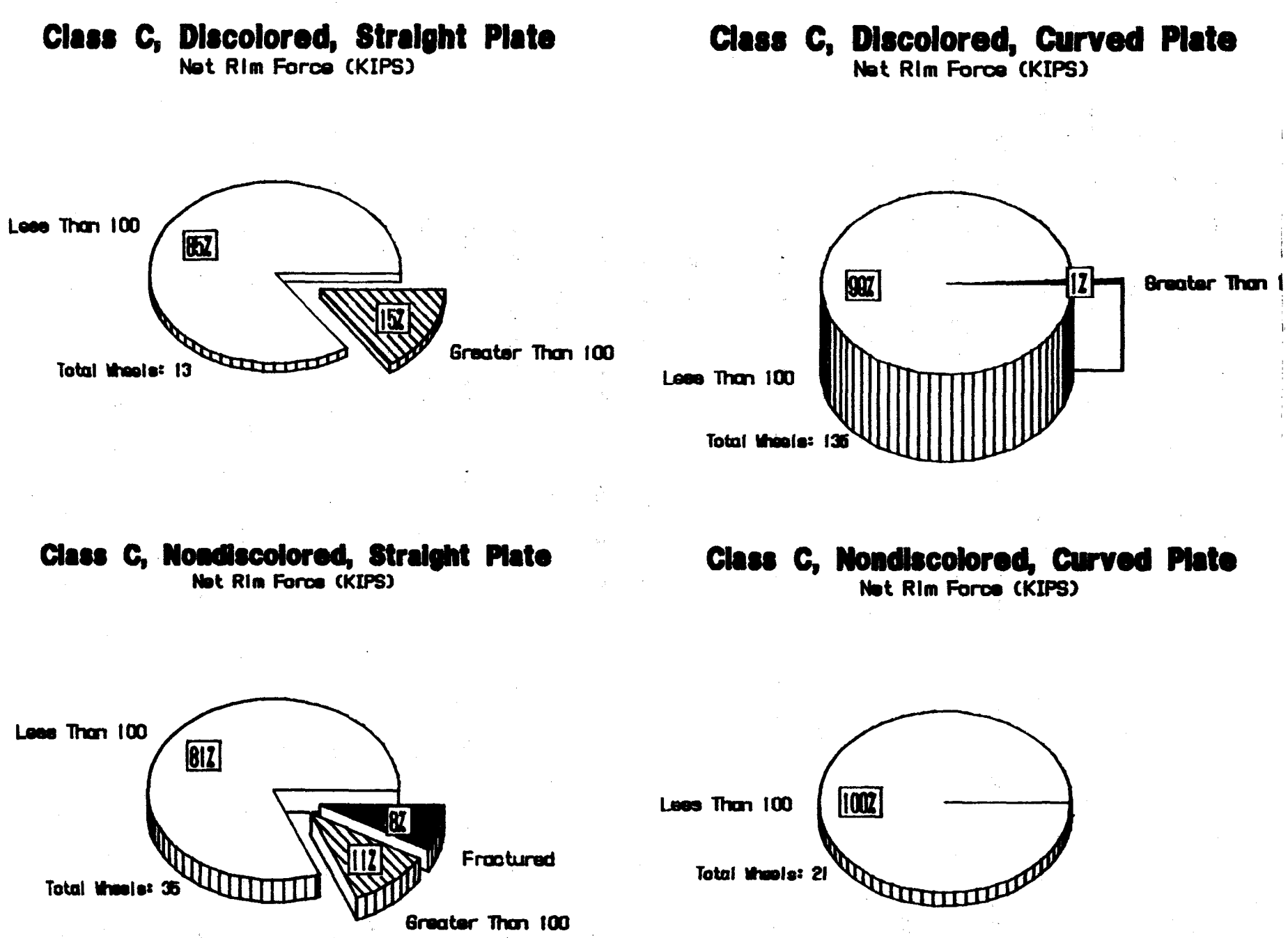

FIGURE 22 NET RIM FORCE BEHAVIOR OF CLASS C WHEELS FROM RAILROAD SERVICE

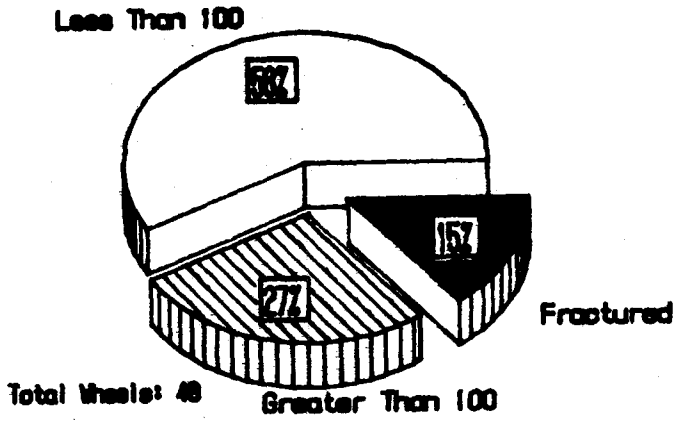

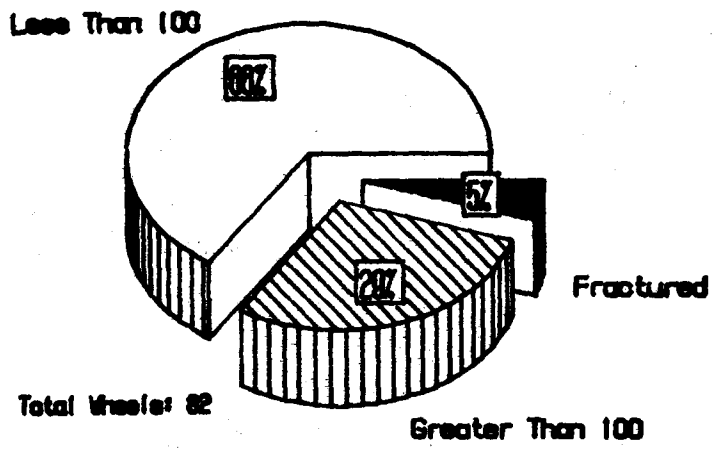

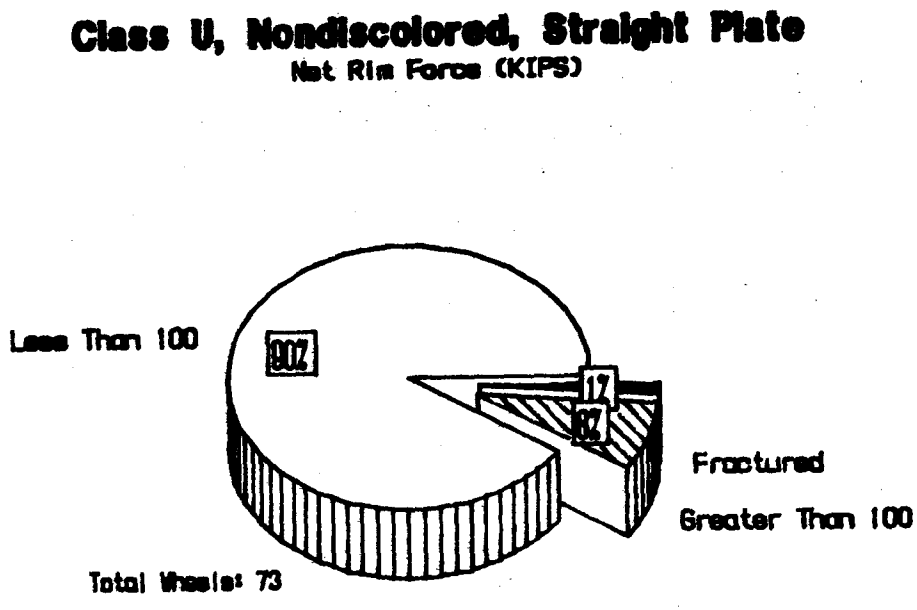

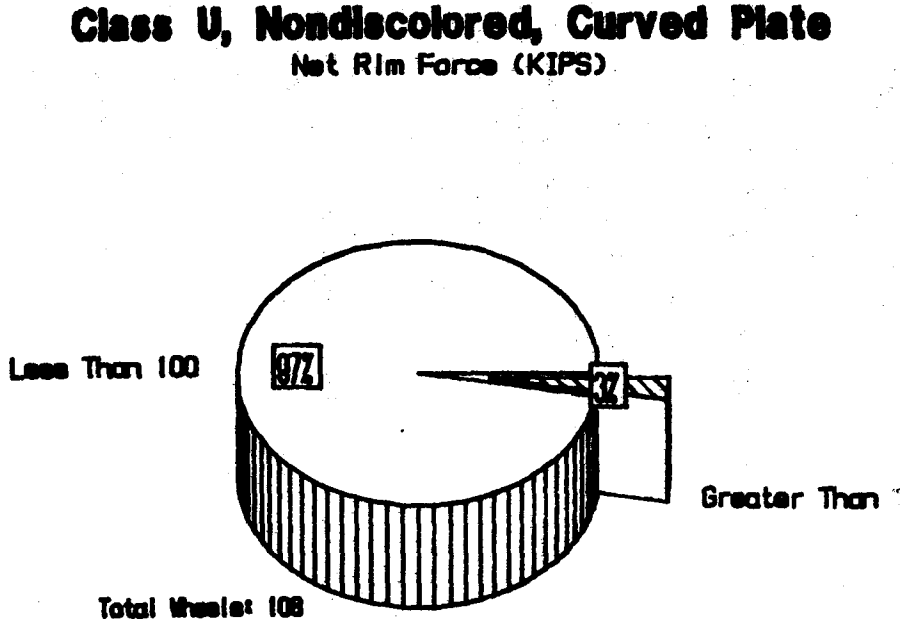

FIGURE 23 NET RIM FORCE BEHAVIOR OF CLASS U WHEELS FROM RAILROAD SERVICE

TABLE 4
DISTRIBUTION OF RIM FORCES FOR SAWCUT SERVICE WHEELS*

**TYPE/DISCOLORATION OF WHEEL
CODE: 1st digit - 1 = curved plate
2 = straight plate
2nd digit - 1 = nondiscolored
2 - discolored

**WHEELS CODE	/CLASS	TOTAL WHEELS	% OF WHEELS <0 kips	% OF WHEELS 0-100 kips	% OF WHEELS >100 kips	% WHEELS WHICH FRACTURED DURING SAW-CUTTING
12	U	82	30.5	40.2	29.9	4.9
22	U	48	41.7	31.2	27.1	14.6
12	C	135	89.6	9.7	0.7	0
22	C	13	84.6	0	15.4	0
12	B	6	66.7	33.3	0	0
11	U	108	51.9	45.3	2.8	0
21	U	73	67.1	24.7	8.2	1.4
11	C	21	95.2	4.8	0	0
21	C	35	74.3	14.3	11.4	8.6
21	B	21	66.7	19.0	14.3	4.8
22	B	5	100.0	0	0	0
11	B	5	100.0	0	0	0

* Data include 27 new wheels.

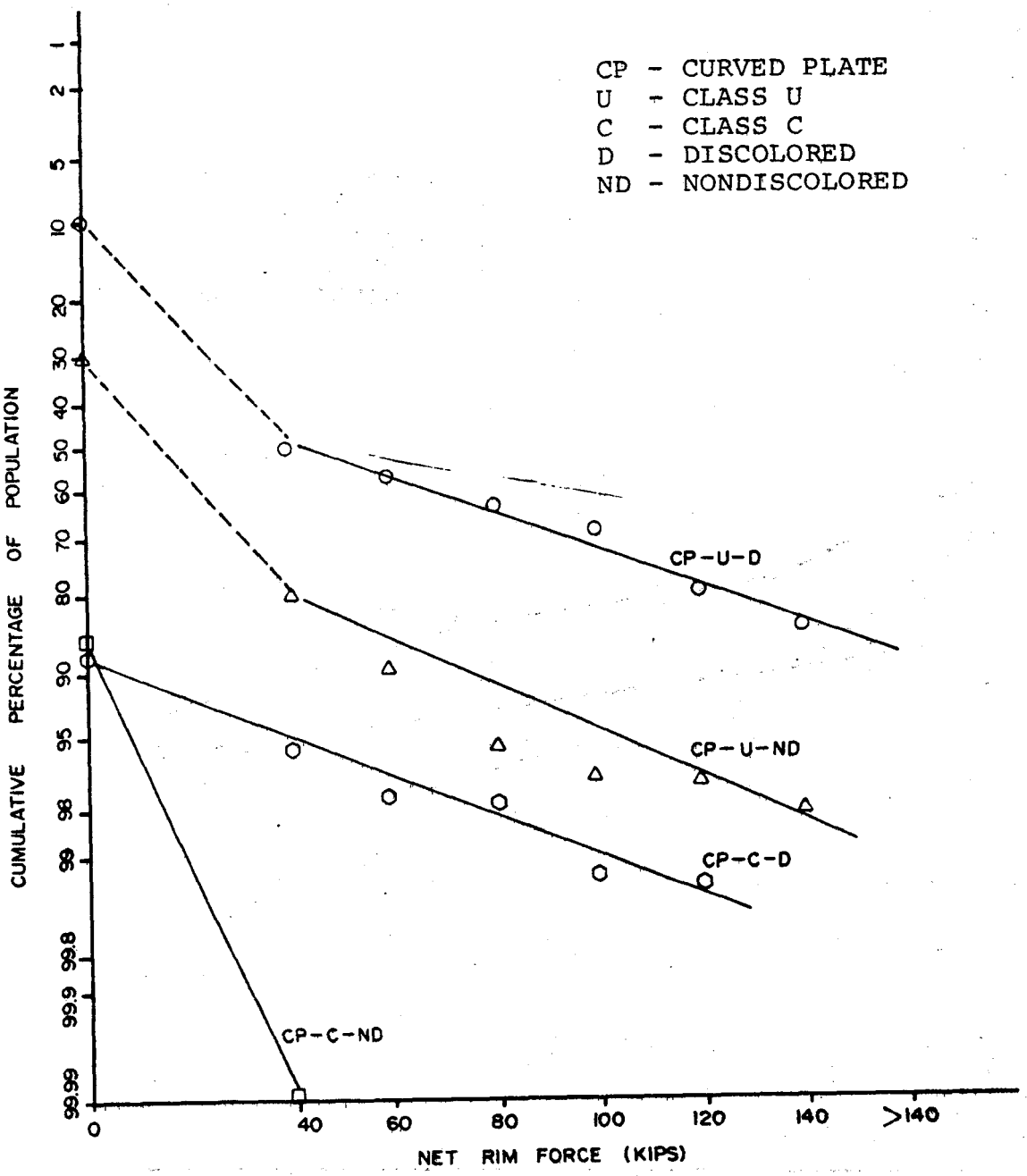

FIGURE 24 CUMULATIVE PERCENTAGE OF CURVED PLATE (SERVICE) WHEEL POPULATION VERSUS NET RIM FORCES COMPUTED FROM SAW-CUT DISPLACEMENT DATA

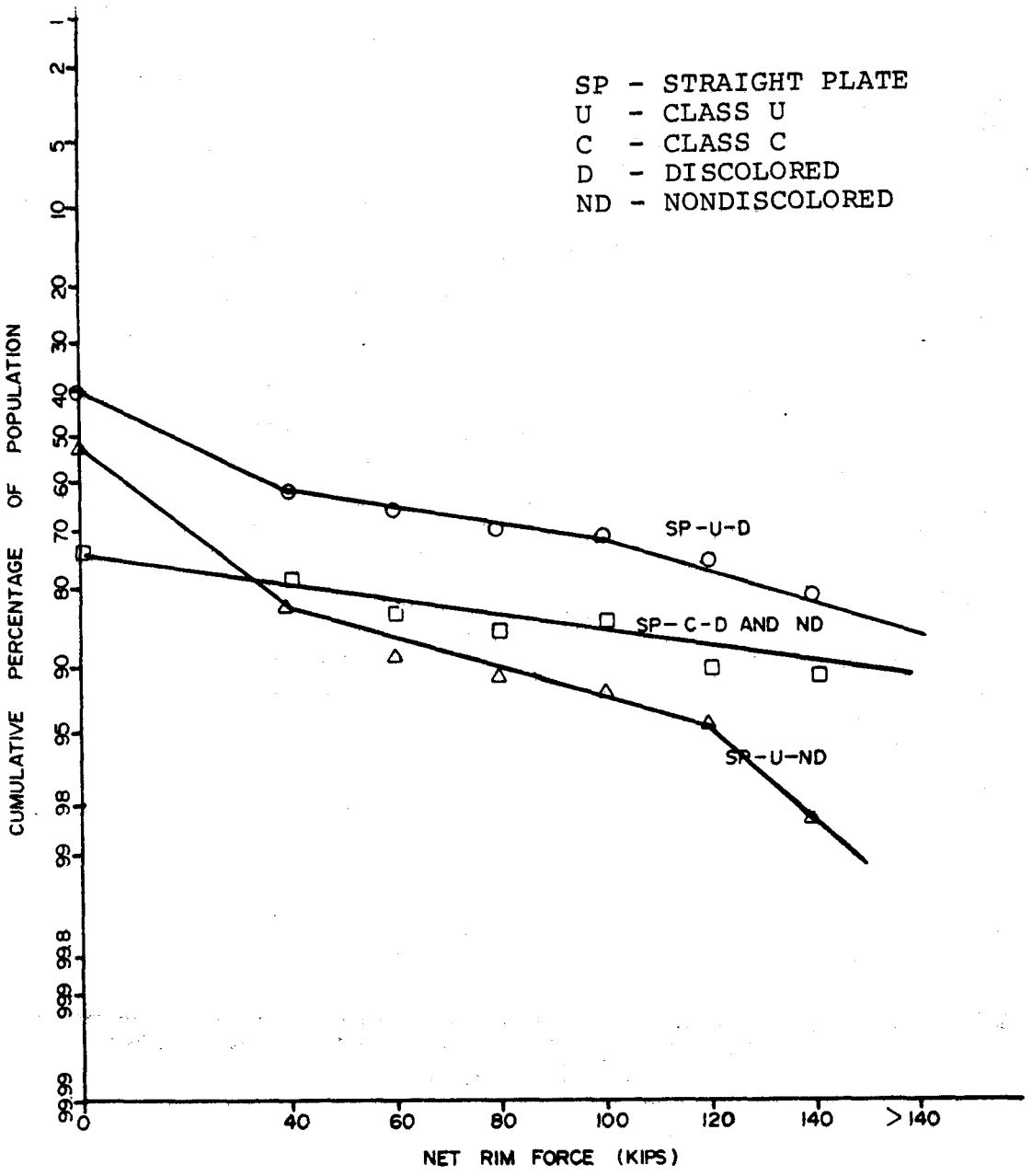

FIGURE 25 CUMULATIVE PERCENTAGE OF STRAIGHT PLATE (SERVICE) WHEEL POPULATION VERSUS NET RIM FORCES COMPUTED FROM SAW-CUT DISPLACEMENT DATA

We see that 73% of these wheels have a net rim force less than 100 Kips.

Sixty wheels with service induced thermal cracks (AAR Code 74) were saw cut. None of these wheels displayed the presence of residual tensile stresses indicating that crack initiation and stress reversal are independent processes. Dynamometer and track test failed to produce thermal cracks in all but one wheel (which required extended and severe drag and stop braking cycles). As all of the wheels tested had new wheel tread profiles, the crack initiation process lacked the necessary mechanical or metallurgical damage to proceed.

3.4 Discussion of Effects of Heat Treatment, Plate Shape, and Discoloration

From the comparison of the relative positions of the cumulative probability lines for the various wheel Subgroups, we can draw some inference about the effect of heat treatment and plate shape on the residual stress.

3.4.1 Effects of Heat Treatment

The most dominant beneficial effect on the residual stresses of service wheels results from heat treatment. A high percentage of Class C wheel population that were saw-cut contained low levels of net rim force.

3.4.2 Effect of Plate Shapes

A higher percentage of curved plate wheels contained lower levels of net rim forces than straight plate wheels.

3.4.3 Effect of Discoloration

Virtually all of the wheels tested on the Roll Dynamics Unit, Brake Dynamometer, and in track testing discolored more than 4-inches. This was to be expected due to the large thermal inputs. During comprehensive track testing, all the test wheels exhibited 4" or more discoloration after 30 drag braking cycles. At that point in testing, only one of the twenty-four wheels showed tensile residual stress on back rim face as measured by hole drilling method. However, the rim force computed from the saw-cut displacement of that particular wheel indicated that it did not contain a net rim tensile stress.

From test data and the results of saw cutting, it was found that it is impossible to estimate the level of thermal damage from the presence of different levels of discoloration.

4.0 ANALYSIS OF DATA FROM TESTS TO PRODUCE RESIDUAL STRESS CHANGES IN TEST WHEELS

The main emphasis of this program was to define operating practices that contributed towards residual stress changes in the wheels, as ascertained by semi-destructive and destructive means of residual stress determination. Information was gathered in different test facilities such as the Brake Dynamometer, Roll Dynamic Unit, and track testing, with

different levels of instrumentation. Although a relatively small number of wheels were used in these tests, they were subjected to closely controlled braking conditions so that complete information on the braking history was available for subsequent analysis. Heavily instrumented wheels were tested on the RDU and in the Preliminary Track Test. Lightly instrumented wheels were tested during Comprehensive Track Tests and on the Brake Dynamometer where nonmeasured conditions were assumed based on the highly instrumented tests. Composition brake shoes were used on all tests.

During RDU and Preliminary Track testing at Pueblo, instrumented brake heads were used, which enabled monitoring of tangential and normal forces at the brake shoe/wheel interfaces on a continuous basis. During Comprehensive Track testing and Brake Dynamometer testing, BHP estimates were made with the assumed average friction coefficient values.

A Braking Severity Index was defined as the cumulative braking energy above threshold horsepower required to cause residual stress changes. This index can be estimated for any combination of speed, brake force, and duration or braking history. It has been established primarily on the basis of the detailed tests and analyses of the reference CJ-33 Class U wheels.

A summary of the rationale and justification for this Braking Severity Index will be given below based on the data

base correlation studies from the several test facilities. This will be followed by an application of the index to provide estimates of the regions of braking operation (speed, force, and duration) that would be expected to produce residual stress changes in various wheel types.

4.1 Development of Braking Severity Index

The brake operation threshold for rim residual stress change can be expressed generically in BHP versus time plot as shown in Figure 26. The representation is similar to that used by the Spanish researchers, Meizoso, and Sevillano in 1985.[8] The BHP history in the various test facilities was reviewed for the test wheels which showed significant residual stress change, and the horsepower-time thresholds were established for curved plate and straight plate wheels, making use of the RDU and track results.

The BHP expended at the interface of brake shoe and wheel tread can be derived from the expression,

$$BHP = \frac{(BSF)(f)(MPH)}{375} \qquad (1)$$

where BSF = Brake shoe normal force in lbs.

f = Coefficient of friction between shoe and tread (average value)

A Braking Severity Index (BSI) can be developed which may be employed to estimate the "threshold" combinations of brake shoe

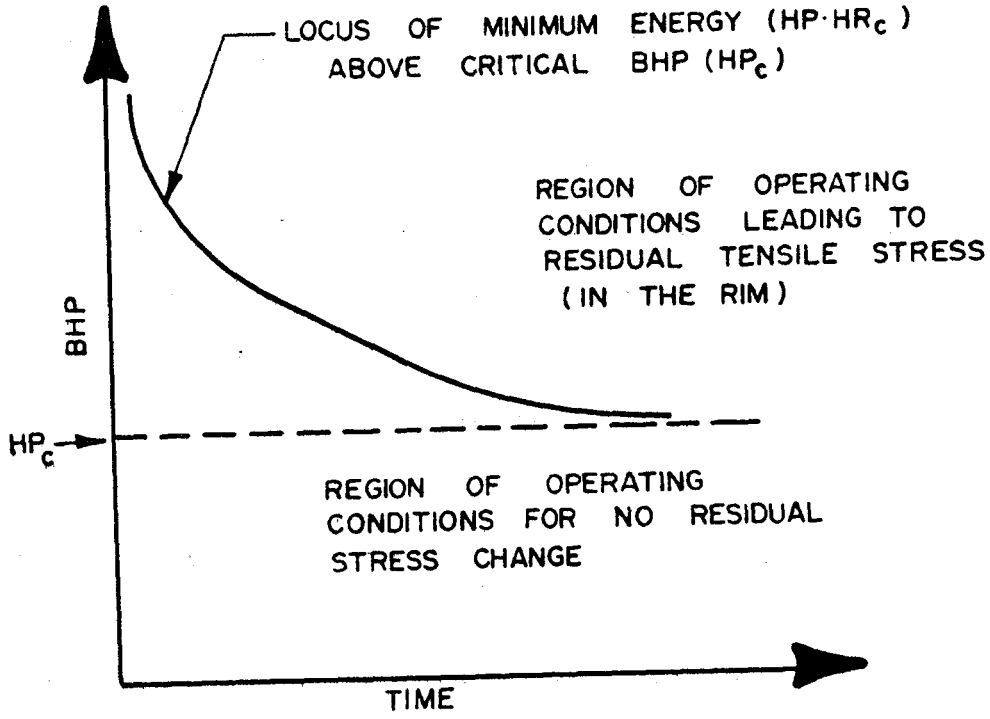

HP_c = CRITICAL BHP LEVEL

FIGURE 26 GENERIC REPRESENTATION OF BRAKING OPERATION SAFETY

force, speed, and duration of drag braking that may be expected to initiate significant change in the rim residual stress.

This Braking Severity Index is defined to be the energy above a critical brake horsepower level (HP_c) that exceeds a minimum required energy (E_c) to cause residual stress change.

$$BSI = (BHP - HP_c)\ HR - E_c$$

Therefore, the "threshold" condition occurs when BSI = 0. The expression for horsepower at this threshold is:

$$BHP = (E_c/HR) + HP_c \qquad (2)$$

4.2 Analysis of the RDU and Preliminary Track Test Data for the Class U, CJ-33 Wheel.

Table 5 presents the details of severe braking episodes which resulted in significant residual stress changes in the test wheels (all Class U, CJ-33, curved plate wheels) during RDU and Preliminary Track testing. The table shows the maximum back rim temperatures attained, peak and average brake horsepower levels during (and prior to) the particular tests, peak hoop (hot) stress measured at the back rim face, the yield ratio at the peak hoop (hot) stress (ratio of peak hoop stress, and the yield stress of Class U steel at the corresponding peak temperature), energy input (E_c) above 40 and 45 BHP, and the change in the residual hoop stress at the back rim face as determined by hole drilling methods (after cooling).

TABLE 5
MEASURED BACK RIM FACE TEMPERATURES AND BHP'S FROM RDU AND PRELIMINARY TRACK TESTING

BI TEMPERATURES, PEAK AND AVERAGE BHP'S, AND PEAK HOOP STRESSES FROM RDU AND PRELIM TRACK TESTING

WHEEL NUMBER	RUN NUMBER	MAX. BI TEMP. PRIOR TO TEST		MAX. BI TEMP. DURING TEST		MEASURED BHP AVERAGE		MEASURED BHP PEAK		ESTIMATED BHP, AVERAGE		PEAK HOOP HOT STRESS (KSI) (σ_H)	YIELD RATIO σ_H / σ_Y	ENERGY INPUT (HP-HRS) ABOVE		Δ HOLE DRILL STRESS (MEASURED)
		T.C.	M.S.	T.C.	M.S.	PRIOR TO TEST	DURING TEST	PRIOR TO TEST	DURING TEST	PRIOR TO TEST	DURING TEST			40 BHP	45 BHP	
5	55 / 56	541	—	555	—	31	41	47	53	30	49	−48	1.06	18.3		
	57 / 58	—	—	—	—	—	53	—	59	28	16	−41	.94	22.5		8
6	55 / 56															
	57 / 58															0
7	55 / 56	494	—	622	—	32	31	43	44	29	52	—	—	0		
	57 / 58	—	—	—	—	—	46	—	61	—	32	—	—	12.8		5
8	55 / 56	500	—	701	—	29	49	45	95	32	55	− 64	1.53	19.4		27
	57 / 58	—	—									− 60	1.35			
9	13	682	—	593	—	23	59	47	19	43	44	—	—	2.2		
	15	682	—	645	—	—	—	—	—	47	46	—	—	—		
	31 − 35	—	—	—	—	—	—	—	—	—		-41 -50	.89 -1.06	5 − 10		
10	13	549	—	495	—	41	56	64	67	46	48	—	—	53	11	14
	15	593	557	611	522	—	48	—	73	—	51	—	—	28	3	0
	30 − 35	—	—	579	565	—	—	—	—	—	—	-50 − -63	1.07 − 1.3	35 − 46		0
11	13	570	—	521	—	37	41	56	58	47	49	—	—	27	1	4
	15	570	—	614	—	—	50	—	82	—	52	—	—	34	5	4
	30- 35	—	—	507	—	—	—	—		—		-40 − -42	1.16 − 1.29	37 − 43		0
12	13	540	—	531	—	51	44	92	60	44	47	—	—	24	0	5
	15	635	—	682	—	—	50	—	72	—	53	—	—	45	5	5
	31 − 35	—	—	532	—	—	—	—	—	—	—	—	—	27 − 36		3

TC — THERMOCOUPLE
MS — MICROSCANNER

$\sigma_H / \sigma_{YIELD}$ − YIELD RATIO

WHEELS 5,6,7, & 8 : RDU TESTING
WHEELS 9,10,11, & 12 : PRELIMINARY TRACK TESTING

As can be seen, high hoop (hot) stress and yield ratio occurred with high back rim temperatures, and they also reflect higher levels of BHP expended at the brake shoe/wheel interface. Energy inputs (E_c) above 40 BHP and 45 BHP were computed for the most severe drag braking episodes during RDU and Preliminary Track testing. The effect of major drag braking cycles on residual hoop stress change at the back rim face was examined. The magnitude of critical BHP was different for RDU testing and track testing. It was observed that a certain amount of energy over and above the critical BHP was required to alter the rim residual stress, as ascertained by hole drilling-strain gaging method conducted on all the test wheels. It was observed that higher amounts of BHP levels were required during track testing than during RDU testing to alter the rim residual stresses. This was due to the fact that more heat was carried away due to convection during track testing than it was possible during RDU testing.

The Braking Severity Index (BSI) developed above may be employed to estimate the threshold levels of brake shoe force, speed, and duration of drag braking that may be expected to alter the residual stress in the rim.

In terms of brake shoe force and speed, equation (2) can be rewritten as:

$$BHP = \frac{(BSF)(MPH)(f)}{375} = E_c/HR + HP_c$$

$$(BSF)(MPH) = \frac{375}{f}(E_c/HR + HP_c) \qquad (3)$$

where	HP_C	=	Critical BHP
	E_C	=	Minimum required energy over and above critical BHP to initiate change in residual stress

The values for critical brake horsepower level, HP_C, and minimum required energy, E_C, were estimated from the evaluation of braking histories that caused residual stress changes in wheels tested under laboratory conditions (RDU) and on track (Preliminary Track testing) during the entire test series. A comprehensive tabulation of all the test parameters including HP_C and E_C are presented in Appendices (Section 7.2).

After the complete evaluation of the test data for the 33 inch diameter, curved plate, Class U wheels, the values of critical brake horsepower level HP_C and minimum required energy above HP_C to initiate residual stress change appear to be:

HP_C	=	45	on Track
E_C	=	5	
HP_C	=	40	on RDU
E_C	=	5	

The corresponding values of brake shoe force and speed at various durations of drag braking that satisfy equation (3) can be easily computed by prescribing the threshold values of HP_C and E_C for laboratory and track testing conditions.

It is best to initially express the brake operation threshold for rim residual stress change in a "Power versus Time" plot similar to that used by Meizoso and Sevillano. Figure 27 presents a reasonable brake severity threshold in the form of "Horsepower-Time Thresholds for Stress Change".* Curve B was estimated to fit the RDU test data, and curve D was estimated to fit Preliminary Track testing data for curved plate, Class U, 33 inch diameter wheels. The difference between curved plate wheels (D) and straight plate wheels (C) was established by judgment from the Comprehensive Track Test data. The critical BHP, HP_c, for straight plate wheels seems to be 35, and the minimum required (threshold) energy over and above HP_c to initiate stress change in the rim is 5 HP-HR.

The corresponding values of brake shoe force and speed at various durations of drag braking were evaluated for the RDU with a criterion of 5 HP-HRS above a 40 HP (threshold), to initiate a significant change in rim residual stress. The values of brake shoe force versus speed for four sets of drag braking durations are presented in Figure 28.

Similar threshold braking cycles were evaluated for track testing conditions, with a criterion of 5 HP x HRS above a 45 (threshold) HP and the corresponding brake shoe forces versus speed at four drag braking durations are presented in Figure 29.

---

*However, this test threshold may not reflect the most adverse braking conditions encountered in actual service where abnormal braking force distribution and shoe placement may occur.

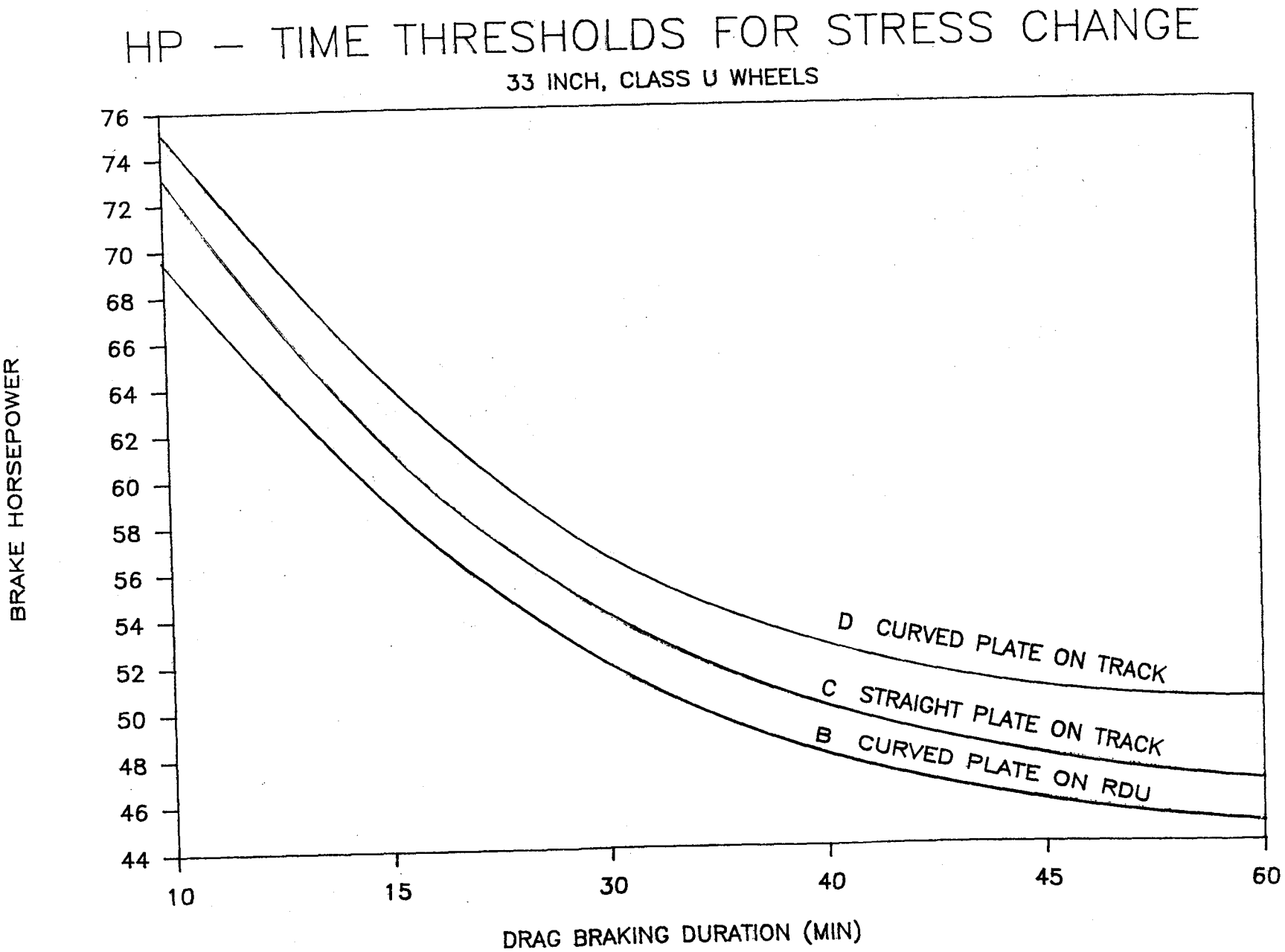

FIGURE 27 HORSEPOWER-TIME THRESHOLDS FOR RIM RESIDUAL STRESS CHANGE

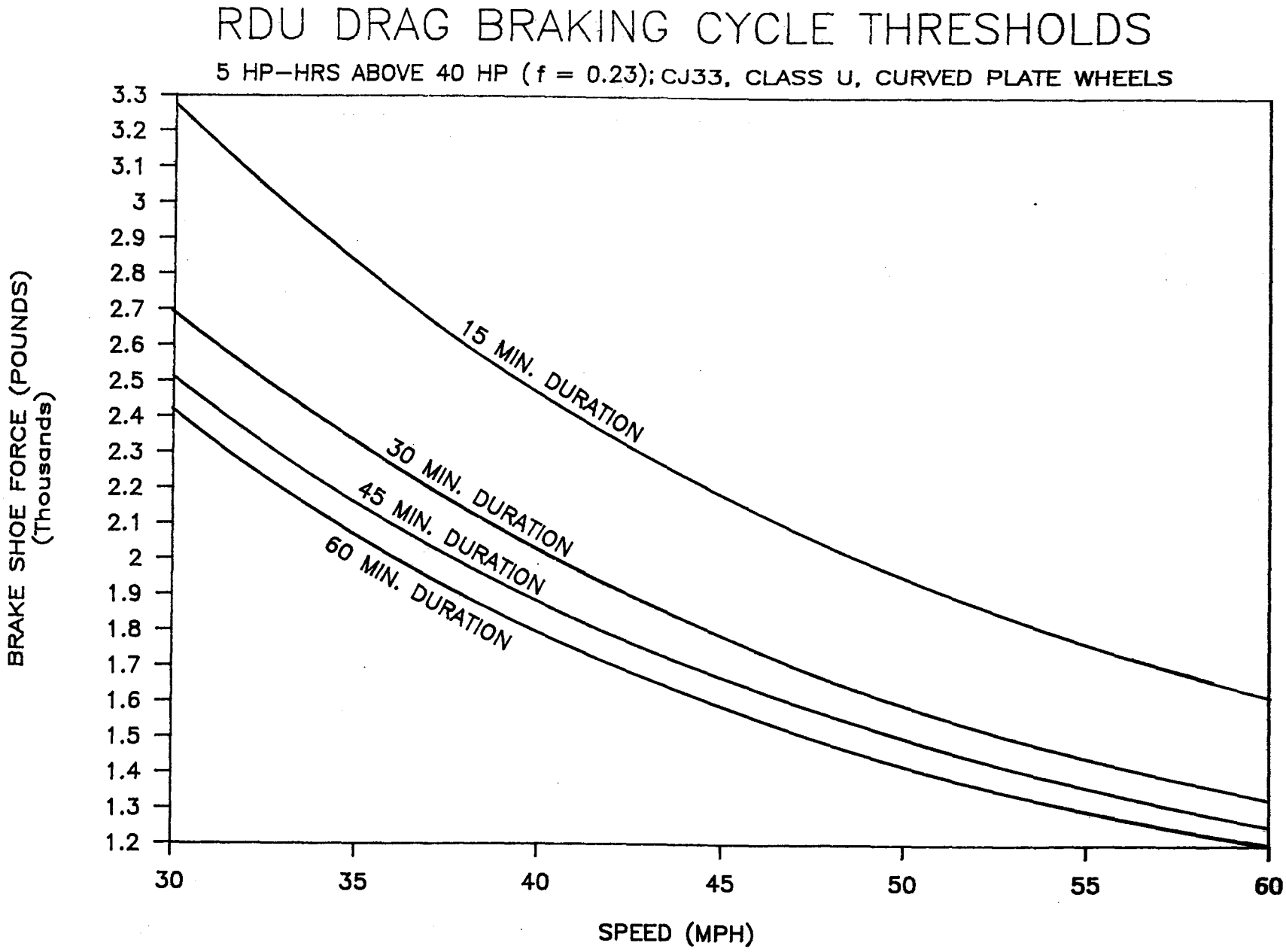

FIGURE 28 THRESHOLD DRAG BRAKING CYCLES ON RDU FOR RIM RESIDUAL STRESS CHANGE IN CURVE PLATE WHEELS

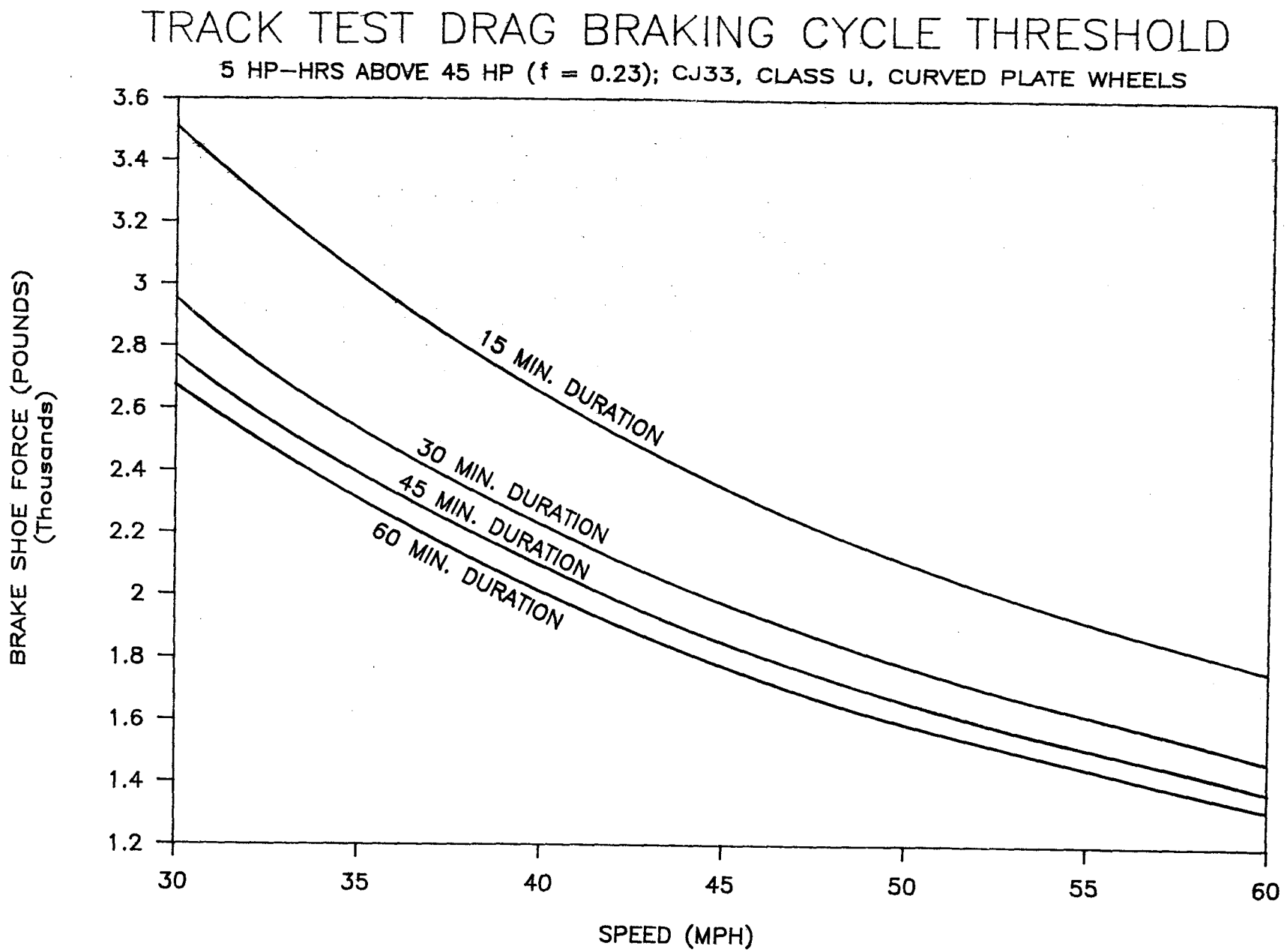

FIGURE 29 THRESHOLD DRAG BRAKING CYCLES ON TRACK FOR RIM RESIDUAL STRESS CHANGE IN CURVED PLATE WHEELS

The threshold brake shoe forces versus speed for 33 inch straight plate, Class U wheels on track, with a criterion of 5 E_c above a 35 HP (threshold) are presented in Figure 30.

Figure 31 presents the threshold loci of BHP versus braking duration for both curved plate and straight plate designs of Class U, 33 inch diameter wheels.

5.0 THERMAL LOAD & BRAKING SYSTEM VARIABILITIES

5.1 Wheel to Wheel Braking Variabilities Seen in Various Test Facilities

Wheel to wheel braking variabilities were observed during several tests conducted on the Brake Dynamometer (Chicago), the Roll Dynamics Unit, and the Transit Test Track at Pueblo. At each facility, the braking forces as well as the effect of braking on the thermomechanical response of wheels were studied.

Special brake heads and load cells were used in the RDU and track tests to measure normal and tangential dynamic-braking forces. This scheme was used previously during the Peotone and Pueblo brake shoe tests. Measurements of the tangential braking force allowed computation of brake horsepower directly.

For the dynamometer tests, the special brake heads and load cells were not used. Instead, the normal braking force was obtained from measurements of brake-cylinder pressure. In a few cases, the tangential braking force was determined from measurements of the torque in the axle supporting the wheel. Inasmuch

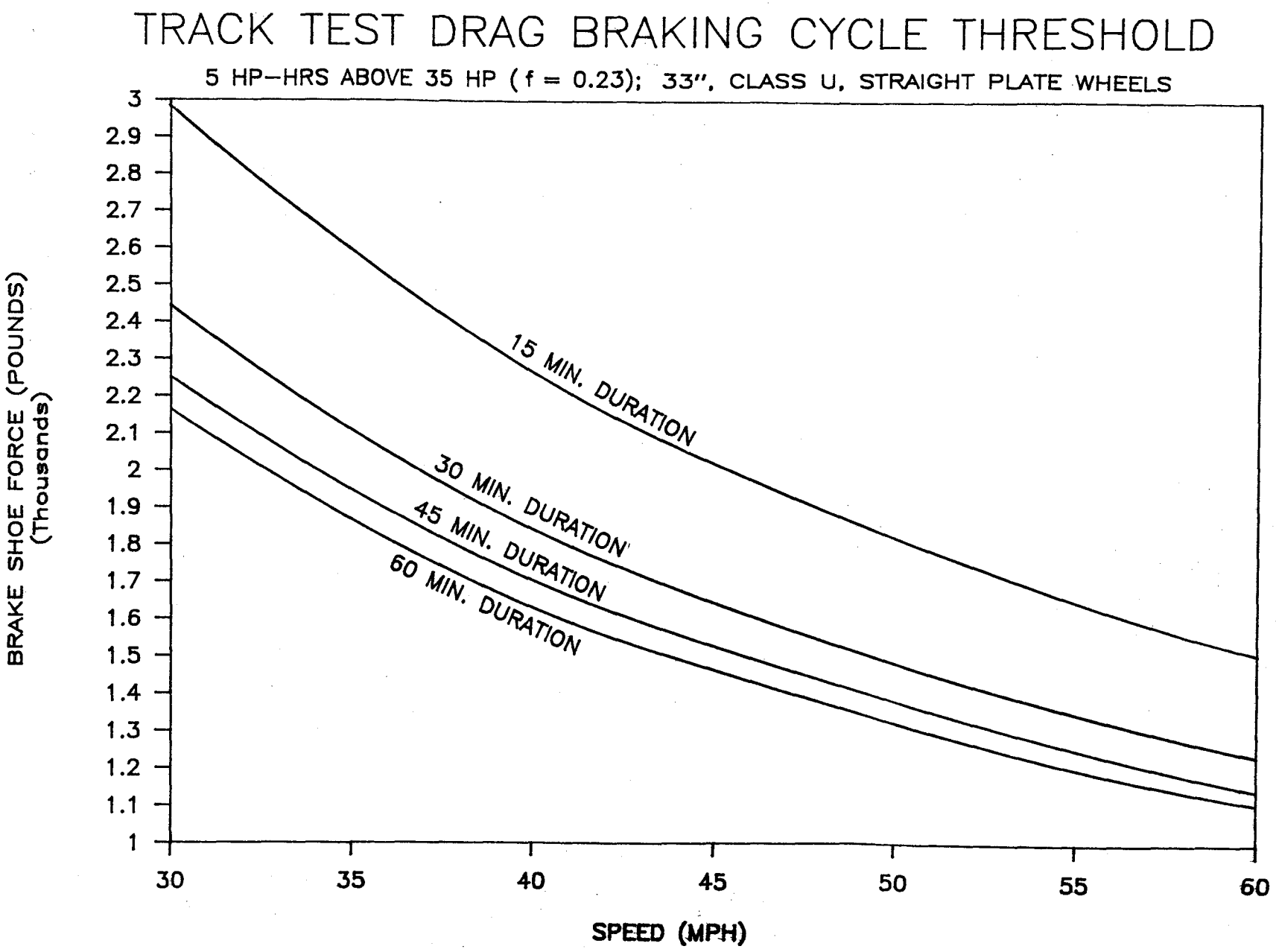

FIGURE 30 THRESHOLD DRAG BRAKING CYCLES ON TRACK FOR RIM RESIDUAL STRESS CHANGE IN STRAIGHT PLATE WHEELS

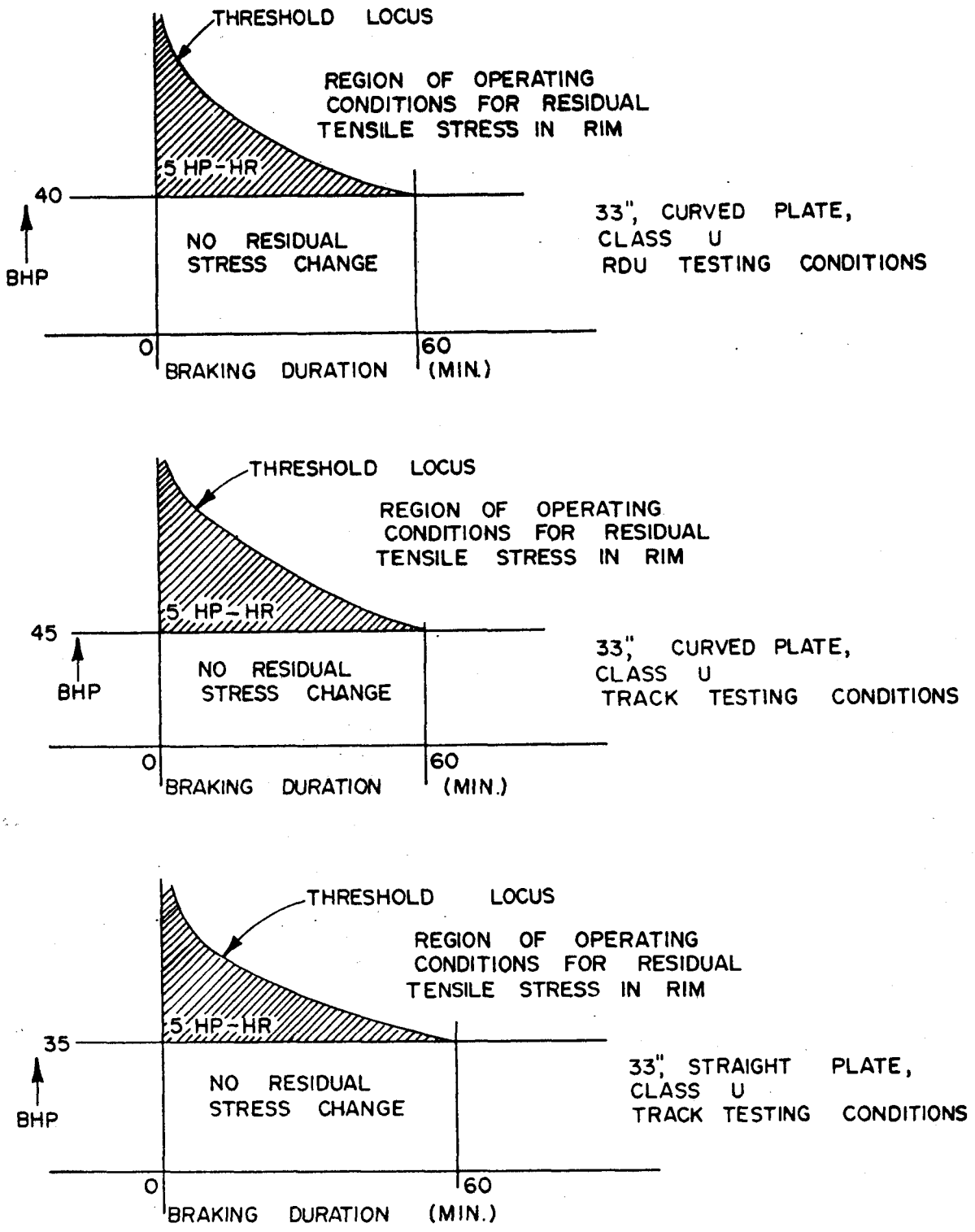

FIGURE 31 THRESHOLD LOCI OF BHP VERSUS BRAKING DURATION FOR 33", CLASS U WHEELS UNDER DIFFERENT TEST CONDITIONS

as the axle torque results from resistance of the track wheel, as well as from the braking forces, torsion values obtained without braking were subtracted from those obtained with braking to obtain the values caused by braking alone. In most of the tests, the axle torque was not measured; the tangential braking force was estimated by using a coefficient of friction value of 0.3.

Temperatures of the railroad wheels, dynamometer rail wheel, RDU supporting rollers, and rails were measured with thermocouples and appropriate recording devices, hand-held infrared thermometers, and a thermal video system.

The thermocouple styles varied, depending on the test facility, the particular experiment being conducted, and the location on the wheel. For tread surface-temperature measurement, several styles of bow-type sliding thermocouples were used for the dynamometer, RDU, and preliminary track tests; thermocouples imbedded in the brake shoes were used in the track tests. Rim and plate thermocouples were bolted or welded to the wheel.

During drag braking tests, temperatures were monitored at the critical locations on the test wheels. The coefficient of friction and bhp levels at the brake shoe-wheel interface were computed from the strain gage data of the instrumented brake heads.

The most important results of the RDU and Preliminary Track testing were the significant wheel to wheel variation in the thermal input, the changes with time in coefficient of friction

of the brake shoes, and the inability to hold a constant level of thermal input to the wheels.

During the drag braking tests, temperatures were monitored at three critical locations of the test wheels (back rim region, back rim fillet region, and front hub fillet region). The coefficient of friction and bhp levels at the brake shoe-wheel interface was computed from the strain gage data of the instrumented brake heads. Maximum level of coefficient of friction, and hence bhp, were attained during the start of the runs, and those values generally decreased (with increase in temperature) toward the end of the braking cycle.

Figure 32 shows the maximum and minimum bhp levels (at the beginning and end of the different duration braking cycles) attained during Truck #1 testing on the RDU for wheels 1, 2, 3, and 4 operated in different directions.

The brake horsepower histories for a severe braking cycle from the RDU and track test program are illustrated in Figure 33. In these cases, both speed and brake shoe forces were increased in order to achieve and sustain the high levels of horsepower shown.

These values were calculated from retarding force measurements directly from the instrumented brake heads.

The wheel thermal response to the severe RDU and Preliminary Track tests is indicated in Figure 34. The back rim face temperature variations are presented. The variability of wheel temperature from wheel to wheel in the same truck and test reflects the variability illustrated in horsepower.

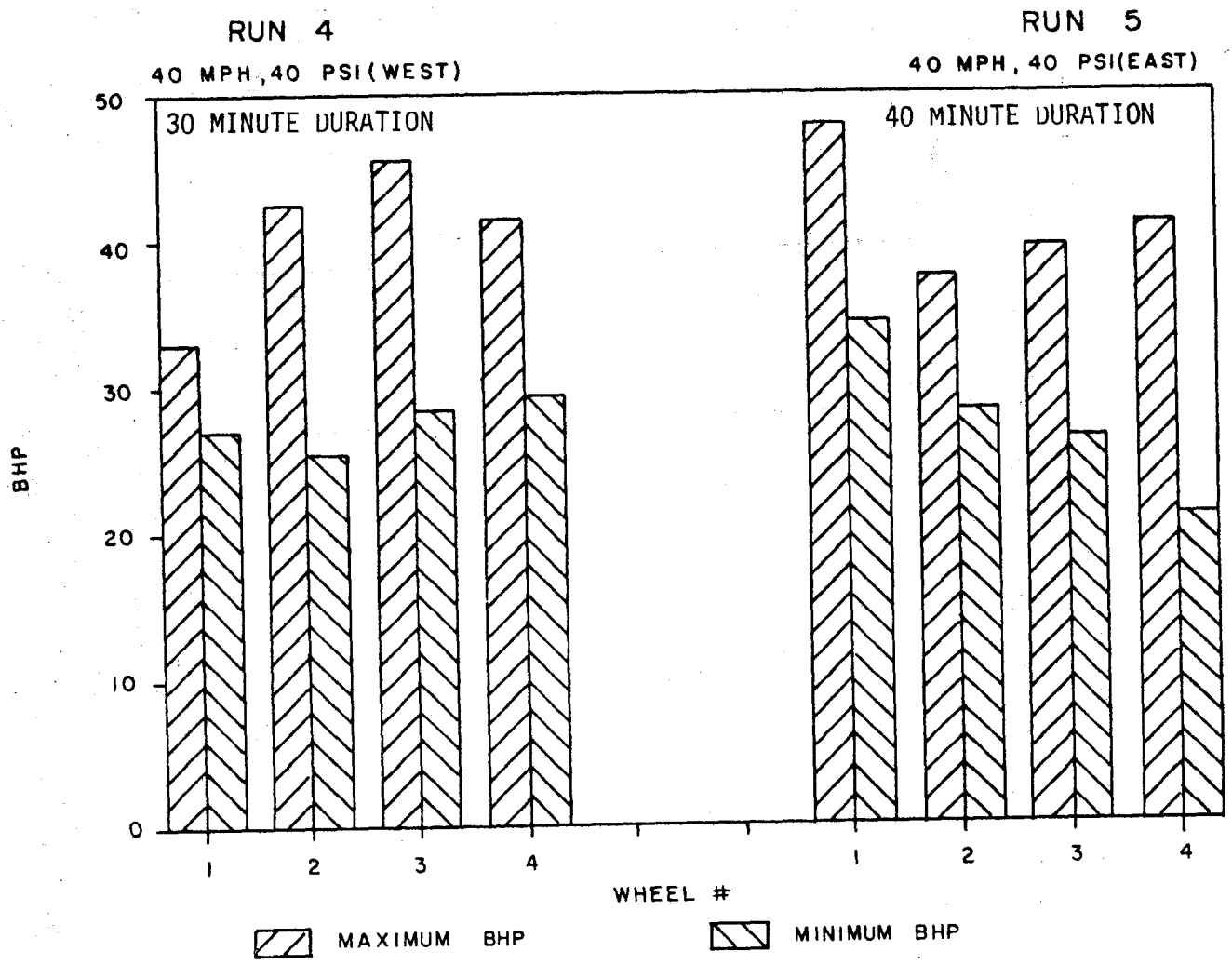

FIGURE 32 MAXIMUM VALUES OF BHP AT BRAKE SHOE/WHEEL INTERFACE FOR WHEELS # 1, 2, 3, AND 4 (TRUCK 1) DURING DRAG BRAKING CYCLES

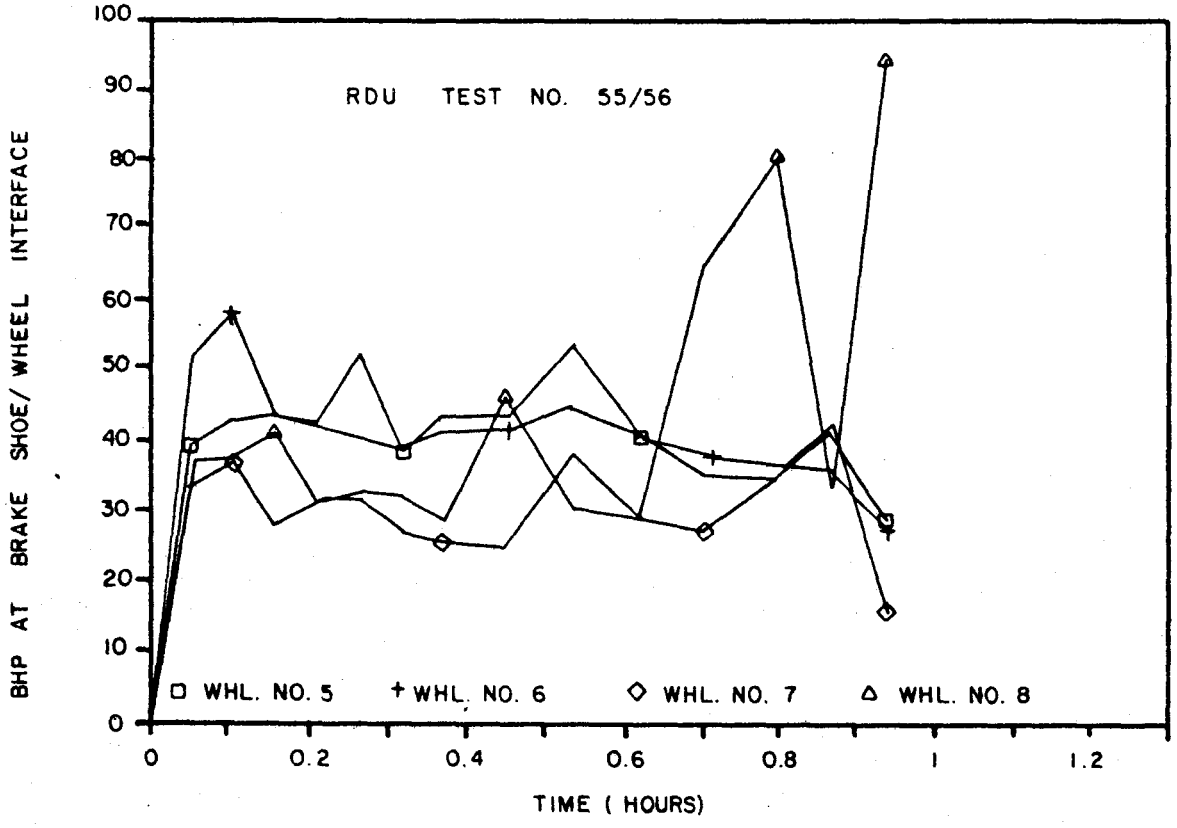

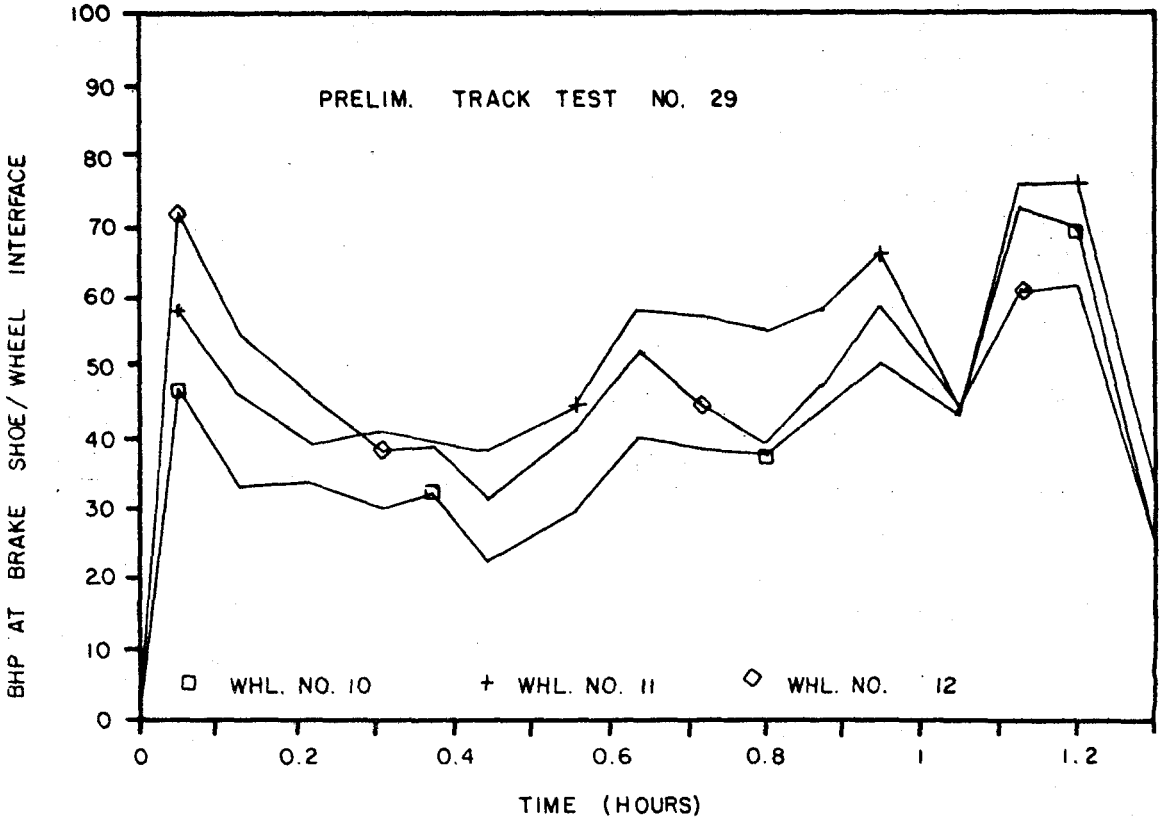

FIGURE 33 BRAKE HORSEPOWER VARIATIONS DURING DRAG BRAKING ON RDU AND TRACK

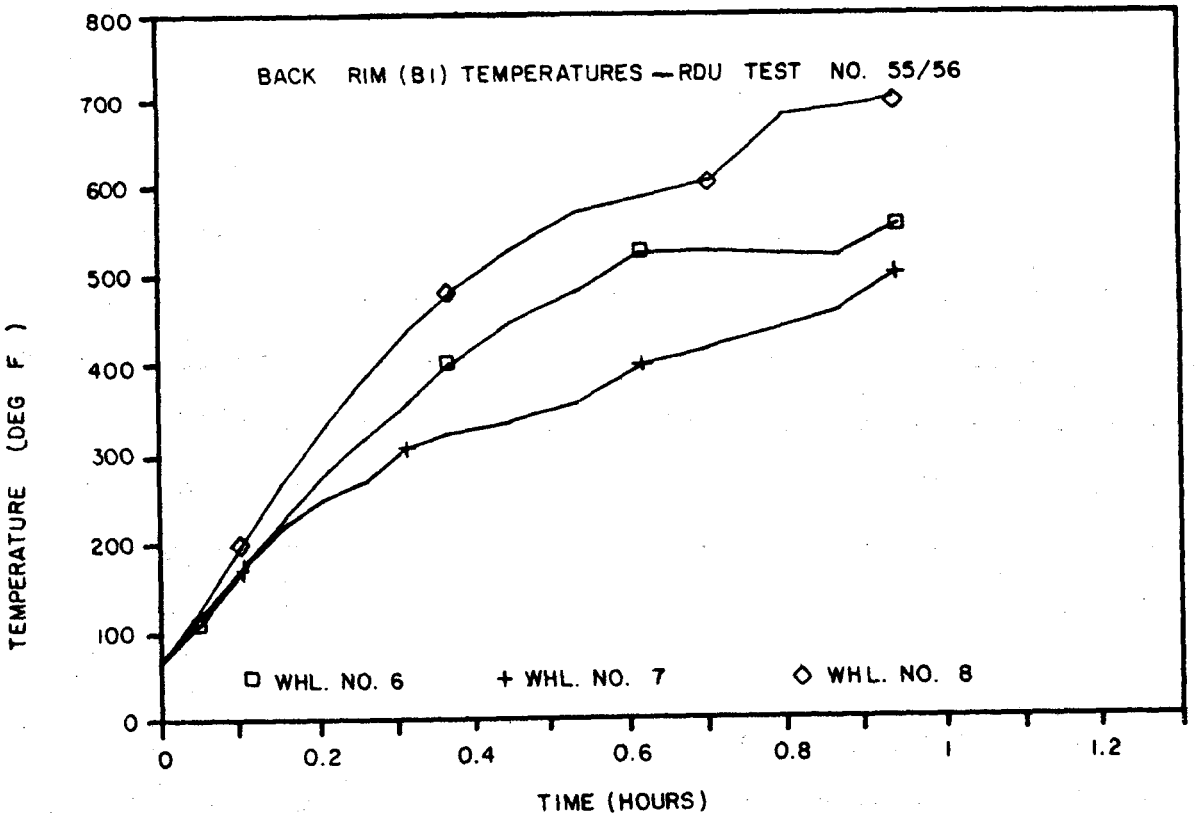

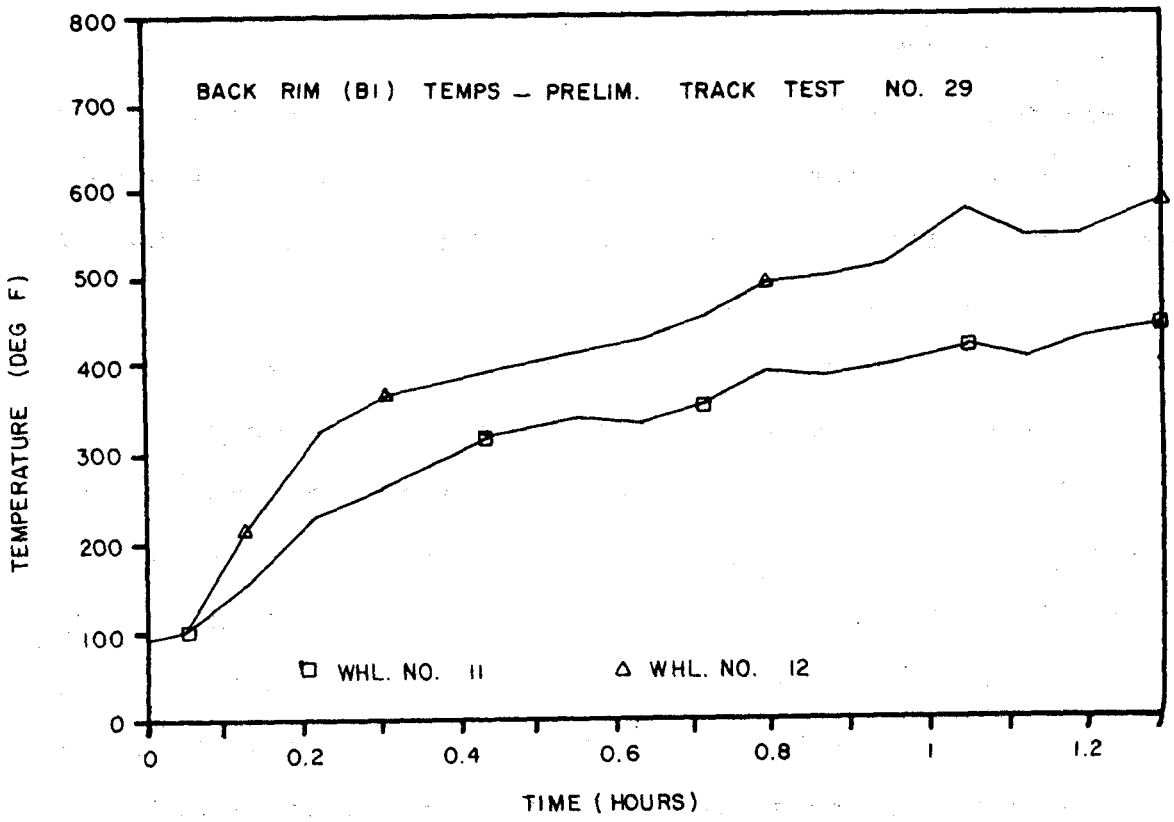

FIGURE 34 TEMPERATURE DEVELOPED ON BACK FACE OF RIM DURING DRAG BRAKING ON RDU AND TRACK

Note the high BHP (top of Figure 33) and back rim temperature (top of Figure 34) measured on wheel #8 at the end of the test. The friction heating was so intense that a brake shoe fire started at this location. Subsequent measurements of residual stress at the back rim location using the hole drilling method revealed that this severe braking cycle caused a large change in residual hoop stress from slightly compressive to 27 ksi tension.

5.2 Nonuniform Heating of Wheels

Special infrared thermographic studies were made of the distribution of temperatures across and around the tread of dynamometer-braked wheels and around the rim and plate of wheels tested on the TTC tracks.

Heretofore, it was assumed that brake-shoe friction would result in an axisymmetric distribution of temperature around the wheel, except for localized transient "hot spots" on the tread surface. However, we noted in our studies that in several cases, the temperature was not uniform around the circumference of the wheels. For example, temperature differences around the tread of up to 200^{o}F. deg. were observed during drag braking.

After a one-hour drag-brake test on TTC tracks at 40 m.p.h. with a consist of two cars of 70-ton capacity and one of 100-ton capacity, the train was brought to a stop using locomotive brakes after the car brakes had been released, and was slowly rolled past the infrared thermographic camera stationed at

trackside. Significant variation in temperature was noted around the rim of several wheels, including the wheel on the trailing axle of the last car (the car of 100-ton capacity). As an example, the description of nonuniform heating of a specific wheel is presented below. The wheel came to a stop at the camera location and the crosshair was moved around the front face rim in a time period of less than one minute at a radius approximately equal to that for the B1 reference location on the back face rim. The highest digital temperature recorded was 642.5 F. deg. at about the 9 o'clock position on the rim, while the lowest was 502.5 F. deg. near the 5 o'clock position.

Therefore, the temperature varied 140 F. deg. over this rim sector of about 120 degrees. This 36-inch parabolic-plate wheel was on an axle of a car with individual brake cylinders for each axle and should have received a nominal 2,600 lbs. of brake force.

5.3 Different Thermal Environments in Various Test Facilities

The thermal environments in various test facilities were studied by estimating the effective braking-power input, taking into account heat-transfer losses at the wheel's interfaces with the rail (conduction), the air (convection) and the brake shoe.[9] Elaborate observations and engineering analyses of such losses from the heated tread were performed based on special heat-transfer tests on the Brake Dynamometer, the Roll Dynamic Unit, and the Transit Track.

Transient and steady rail heat-up measurements indicate heat losses of 18% from rail contact (conduction). Convection heat losses, a function of relative air speed and temperature amounted to 10% at vehicle speeds of 50 m.p.h. Radiation losses from the tread are strongly dependent on the exposed tread temperature with 5% heat loss being typical. Average heat losses of 2% are calculated in the composition brake shoe during drag-braking track tests estimated from the measured temperature gradients within the brake shoe depth. The typical total heat-transfer losses at the wheel's interfaces with the rail (conduction), the air (convection and radiation) and the brake shoe amount to 35%.

5.4 Effect of Brake Shoe Position

An elasto-plastic finite element analysis has shown the brake shoe position has an equally important role in developing residual tensile stresses.[10]

The results of the calculations are summarized in Table 6, where the maximum temperatures, the back rim face, and maximum tread circumferential stresses, both at the end of the 60-minute heating period and after the wheel has cooled, are tabulated.

From a practical standpoint, the high tread tensile residual stresses developed by braking would be modified on the surface by the action of the high contact stresses between the wheel and the rail. Wheels that roll on a rail eventually develop compressive circumferential stress on the tread. Hence it is

TABLE 6
CALCULATED RIM CIRCUMFERENTIAL IN ONE-WEAR WHEELS AFTER ONE HOUR HEATING

Wheel Size [in.(mm)]	Plate Design	Power Input To Wheel [bhp(kw)]	Maximum Temperature [°F(°C)]	Brake Shoe Position	Circumferential Stress at Indicated Locations			
					Bottom of Back Rim		Maximum on Tread	
					Hot [ksi(MPa)]	Residual [ksi(MPa)]	Hot [ksi(MPa)]	Residual [ksi(MPa)]
36(914)	Curved	48(35.8)	1301(705)	Overhang	-49(-338)	21(145)	-28(-193)	43(296)
			1078(581)	Center	-46(-317)	22(152)	-38(-262)	13(90)
			1006(541)	Override	-44(-303)	20(138)	-37(-255)	33(228)*
36(914)	Straight	48(35.8)	1268(687)	Overhang	-41(-283)	25(172)	-35(-241)	49(338)
			1083(584)	Center	-39(-269)	17(117)	-41(-283)	38(262)
			1043(562)	Override	-37(-255)	4(28)	-36(-248)	40(276)
33(838)	Curved	43(32.1)	1257(681)	Overhang	-46(-317)	20(138)	-29(-200)	44(303)
			1064(573)	Center	-43(-296)	21(145)	-40(-276)	18(124)
			1022(550)	Override	-41(-283)	18(124)	-36(-248)	31(214)*
33(838)	Straight	43(32.1)	1306(708)	Overhang	-42(-290)	30(207)	-37(-255)	49(338)
			1103(595)	Center	-42(-290)	20(138)	-39(-269)	39(269)
			1035(557)	Override	-40(-276)	8(55)	-38(-262)	39(269)
28(711)	Curved	37(27.6)	1314(712)	Overhang	-41(-283)	1(7)	-26(-179)	42(290)
			1112(600)	Center	-33(-228)	2(14)	-30(-207)	8(55)
			1051(566)	Override	-22(-152)	4(28)	-30(-207)	18(124)*
28(711)	Straight	37(27.6)	1285(696)	Overhang	-40(-276)	33(228)	-38(-262)	48(331)
			1090(588)	Center	-41(-283)	22(152)	-39(-269)	45(310)
			1048(564)	Override	-39(-269)	5(34)	-38(-262)	45(310)

*Indicates that the maximum stress occurred on the flange.

Note: With an overhanging brake shoe, the heat is put into the rim from the same node near the front face as in the centered brake shoe to a distance 1-11/16 inches (43 mm) away. With an overriding brake shoe, heat is put into the rim from the tip of the flange to a distance 3-3/8 inches (86 mm) away on a uniform longitudinal basis.

believed that these high stresses would not contribute to the initiation and propagation of thermal cracks on the tread surface.

The overriding brake shoe leads to high residual stresses in the flange. These high stresses could lead to the development and growth of surface flange cracks, which are an important mode of failure in 33 in. diameter Class U wheels.[11]

Note that all three straight-plate designs have about 40 ksi compressive hot circumferential stresses, regardless of the location of heat input. The larger curved-plate wheel designs show lower tread stresses for the overhanging brake shoe case, but the hot stresses in the other two cases are also close to 40 ksi. The 28 in. diameter S-plate design usually shows much lower hot stresses.

There is a significant difference in residual stress patterns between the straight-and curved-plate designs. With the straight-plate design, the highest residual stress on the back rim face results from an overhanging brake shoe. With the curved-plate design, the residual stress at the bottom of the back rim face is almost constant, regardless of brake shoe location.

The largest residual stresses have been predicted for the straight-plate 28 in. diameter wheel design. This wheel type had a very poor service record and has been banned.

6.0 NONDESTRUCTIVE EVALUATION TECHNIQUES

The main objective of this task was to review and evaluate nondestructive testing techniques for isolating cracked or critically stressed wheels. Initially, an investigation of promising methodologies was made through discussions and marketing literature, followed by a critical literature review and selection of one of the crack detection or residual stress measurement prototypes for evaluation.

The test plan required critical review and selection of one NDE (either crack detection or stress measurement) prototype, followed by limited testing and evaluation of this one device in support of appropriate program tasks at TTC. Those techniques reviewed were X-ray diffraction, Barkhausen Methods, ultrasonic bi-refringence, magneto-mechanical acoustic emission, and magnetic/ultrasonics for residual stress detection. Crack detection techniques reviewed were ultrasonics and acoustic signature analysis.

Two specific residual stress measurement techniques were pursued by AAR under the Wheel Failure Mechanisms Program.

6.1 Magnetic/Ultrasonic Technique for Residual Stress Measurement

Magnetic/ultrasonic technique for residual stress measurement developed by NASA, Langley, is the most promising method due to its bulk stress measurement capability combined with the absence of elaborate calibration requirements.

A joint effort involving AAR, FRA, and NASA has resulted in the assembly of a test system which employs the magneto-acoustic technique to nondestructively determine the residual stress state in railroad wheels.

After successful completion of this lab-oriented phase of the project, two large electromagnet assemblies were built and tested to be both maneuverable and powerful enough to supply a strong magnetic field in wheel rims, and the entire technique was successfully performed using two different computer systems.

The NDE effort covered under the Wheel Failure Mechanisms Program was limited to making available a prototype device in collaboration with NASA, Langley. This device is capable of making stress measurements in the rim of a full scale railroad wheel.

6.2 Ultrasonic Bi-Refringence Technique for Residual Stress Measurement.

Significant progress has been made in the usage of the electro-magnetic acoustic transducer (EMAT) in the Bi-Refringence technique at the National Bureau of Standards in Boulder, Colorado. The device is applied to the back rim face of a railroad wheel and orthogonally polarized shear horizontal waves are propagated through the thickness of the wheel rim. The difference in arrival times (Bi-Refringence) is related to the difference in principal stresses. TTC maintained contact

with NBS, Boulder, and supported them by supplying full-size wheels and cut samples of wheels. After successful implementation of this technique using EMAT's on the rims of full-size railroad wheels, this method was used to analyze six wheels which were tested on RDU. The preliminary results of the residual stresses in the rim were very encouraging.

The NDE effort covered under the Wheel Failure Mechanisms Program is limited to the above level, where an ultrasonic Bi-Refringence system using EMAT's is available at NBS, Boulder, capable of making stress measurements in the rim of a full scale railroad wheel under laboratory conditions.

7.0 CONCLUSIONS

1. Class C wheels are better than Class U wheels vis-a-vis stress reversal, and marginally better in crack initiation, and crack growth.
2. Class C wheels are less susceptible than Class U wheels to mechanical damage (harder than standard rail, about same as heat treated rail).
3. If Class C wheels show evidence of mechanical damage, they have been severely abused.
4. The number of all derailments including those due to wheel thermal failure has been decreasing since 1980.
5. Derailments due to wheel thermal failure are highly seasonal with the majority of derailments occurring in the winter months.

6. Wheels fail due to cracks from mechanical damage (i.e., tread metal flow beyond rim face; wear ridge on flange; gouges; metal flow on rim faces), and a combination of service induced stresses and stress reversal due to thermal damage.
7. Stress reversal occurs in curved plate wheels at higher thermal input than in straight plate wheels.
8. Discoloration, while it indicates thermal input, is not necessarily evidence of destructive thermal damage.
9. The saw cut analysis of discolored Class U wheels indicates that 34 percent of the curved plate wheels and 42 percent of the straight plate wheels contain residual stress of sufficient magnitude to cause thermal cracks to grow. Of these wheels, 5 percent of the curved plate and 15 percent of the straight plate wheels have residual stress states that are, alone, sufficient to cause failure in the presence of a significant thermal crack.
10. Almost all (97%) failures of curved plate wheels originate at a sharply worn flange tip.
11. Failures of straight plate wheels originate from mechanical damage at tread, flange, and rim locations.
12. Brake shoes which overhang the front rim face of a wheel are the most likely to impart severe thermal damage according to finite element analysis.
13. Brake heat input may vary from wheel to wheel on the same truck and around the circumference of a wheel.

14. Specific combinations of time, speed, and brake shoe force are required to produce a circumferential residual tensile stress in the wheel rim for each diameter, design, and heat-treatment.

15. For the same thermal input, a new single wear wheel will develop lower tensile stress than a wheel with a condemning rim cross section.

16. No effective nondestructive methods exist, at this time, to efficiently and accurately determine the level of residual stress, but the promising systems are under development.

8.0 REFERENCES

1. D.H. Stone, W.S. Pellini, and W.J. Harris, Jr., "North American Wheel Failure Experience", Third International Heavy Haul Railway Conference, Paper I-18, Vancouver, October, 1986.
2. W.S. Pellini and D.H. Stone, "Analysis of Wheel Fracture Factors by Review of Railroad Reports for Fractures that Resulted in Derailments", AAR Report R-641, June, 1987.
3. C.S. Carter, R.G. Caton, and J.L. Guthrie, "Fracture Resistance and Fatigue Crack Growth Characteristics of Railroad Wheels and Axles", Report DOT-TSC-617, April, 1974.
4. Railway Mechanical Engineering: A Century of Progress, ASME, (New York, 1979), pp. 293-306.
5. H.N. Jones, III, "The Characterization of the Residual Stress State of Railroad Wheels by The Saw Cut Method", ASME Rail Transportation Conference Proceedings, April, 1985, pp. 15-19.
6. M.R. Johnson, R.R. Robinson, A.J. Opinsky, M.W. Joerms, and D.H. Stone, "Calculation of Residual Stresses in Wheels From Saw-Cut Displacement Data", ASME Paper 85-WA/RT-17, November, 1985.
7. S.M. Patil and B.R. Rajkumar, "An Analytical Method for Determining Residual Stresses in Railroad Wheels", Proceedings of the IEEE-ASME Joint Railroad Conference, Toronto, 1987, pp. 115-121.

8. A. Martin-Meizoso and J. Gil-Sevillano, "Thermal: A Computer Code for Life Prediction of Railway Wheels", Proceeding of the Eight International Wheelset Congress", Madrid, 1985, Paper II.2.

9. G.J. Moyar, G.F. Carpenter, and B.R. Rajkumar, "Heat Transfer Experiments with Braked Railcar Wheels", ASME Paper 86-WA/RT-1, December, 1986.

10. A.J. Opinsky, M.W. Joerms, D.H. Stone, and M.R. Johnson, "Effect of Brake Shoe Position on the Development of Residual Stresses in Freight Car Wheels as a Result of Simulated Drag Braking", ASME Paper 85-WA/RT-3, December, 1986.

11. A.J. Opinsky, "An Analysis of Some Railroad Wheel Flange Failures", AAR Report R-571, March, 1984.

12. M.C. Fec and H. Sehitoglu, "Behavior of Railroad Wheel Steels Under Selected Thermal Histories", Proceedings of the Third International Heavy Haul Conference. Vancouver, 1986.

GLOSSARY OF TERMS

Cast Iron Brake Shoe: A brake shoe made of a high phosphorus (0.4 to 3.0 percent) cast iron.

Cast Wheel: A wheel that is manufactured by casting steel into a wholly or partially graphite mold.

Composition Brake Shoe: A brake shoe formed of a rubber, steel powder, and knolin composite adhesively bonded to a steel backing plate.

Crack Initiation: The formation of a crack large enough to grow under alternating stress.

Curved Plate Wheel: A wheel whose plate profile has a fully parabolic shape (see Low Stress Wheel).

Class B Wheel: A wheel which is rim quenched to yield a hardness of 277 to 341 Brinell. Grade B wheels contain 0.57 to 0.67 percent carbon.

Class C Wheel: A wheel which is rim quenched to yield a hardness of 321 to 363 Brinell. Grade C wheels contain 0.67 to 0.77 percent carbon.

Class U Wheel: An unheat-treated wheel which contains 0.65 to 0.80 percent carbon.

Discolored Wheel: A wheel which has a pattern of redish-brown or blue discoloration from heat on the front and back face of the rim, four inches or more into the rim with decreasing intensity.

Fracture: Rapid, unstable growth of a crack at rate approaching the speed of sound.

H-36 or CH-36 Wheel: A 36-inch diameter one-wear wheel for service on 100-ton cars. The C prefix indicates that the wheel is cast whereas the lack of a C prefix indicates a wrought wheel.

High Stress Wheel: A wheel of a design which does not meet the requirements of AAR Standard S-660.

Incremental Crack Growth: The slow, stable growth of a crack by fatigue.

J-33 or CJ-33 Wheel: A 33-inch diameter one-wear wheel for service on 70-ton cars. The C prefix indicates that the wheel is cast whereas the lack of a C prefix indicates a wrought wheel.

J-36 or CJ-36 Wheel: A 36-inch diameter two-wear wheel for service on 100-ton cars. The C prefix indicates that the wheel is cast whereas the lack of a C prefix indicates a wrought wheel.

K_{Ic}: The critical stress intensity factor, or fracture toughness, of a material. K_{Ic} defines the level of stress and crack size.

Low Stress Wheel: A wheel of a design which meets the requirements of AAR Standard S-660 (Finite Element Analysis).

S-Plate Wheel: A wheel whose plate profile has an S shape (see Low Stress Wheel).

Straight Plate Wheel: A wheel whose plate profile has a straight section between the rim and hub filets (see High Stress Wheel).

Thermally Damaged Wheel: Any wheel, which through excessive brake shoe heating, has developed tensile residual hoop stresses in its rim.

Wrought Wheel: A wheel which is manufactured by a process of forging and rolling.